BOLU ABANT IZZET BAYSAL UNIVERSITY
INSTITUTE OF GRADUATE STUDIES

INVESTIGATION OF ANOMALOUS HIGGS-GAUGE BOSON COUPLINGS VIA HVV PRODUCTION AT CLIC

MASTER OF SCIENCE

ÖZGÜN KARADENİZ

BOLU, JULY 2020

BOLU ABANT IZZET BAYSAL UNIVERSITY
INSTITUTE OF GRADUATE STUDIES
DEPARTMENT OF PHYSICS

INVESTIGATION OF ANOMALOUS HIGGS-GAUGE BOSON COUPLINGS VIA HVV PRODUCTION AT CLIC

MASTER OF SCIENCE

ÖZGÜN KARADENİZ

BOLU, JULY 2020

APPROVAL OF THE THESIS

INVESTIGATION OF ANOMALOUS HIGGS-GAUGE BOSON COUPLINGS VIA HVV PRODUCTION AT CLIC submitted by **Özgün KARADENİZ** in partial fulfillment of the requirements for the degree of **Master of Science** in **Physics Department, Institute of Graduate Studies of BOLU ABANT IZZET BAYSAL UNIVERSITY in 24/07/20** by

Examining Committee Members	**Signature**
Supervisor Prof. Dr. Abdulkadir Şenol Bolu Abant İzzet Baysal University	....
Member Prof. Dr. Haluk Denizli Bolu Abant İzzet Baysal University	....
Member Dr. Öğr. Üyesi Ali Yılmaz Giresun University	....

Prof. Dr. Osman Görür ....

Director of Institute of Graduate Studies

To my family

DECLARATION

I hereby declare that all information in this document has been obtained and presented in accordance with academic rules and ethical conduct. I also declare that, as required by these rules and conduct, I have fully cited and referenced all material and results that are not original to this work.

Özgün KARADENİZ

ABSTRACT

INVESTIGATION OF ANOMALOUS HIGGS-GAUGE BOSON COUPLINGS VIA HVV PRODUCTION AT CLIC

MSC THESIS

ÖZGÜN KARADENİZ,

BOLU ABANT IZZET BAYSAL UNIVERSITY

INSTITUTE OF GRADUATE STUDIES

DEPARTMENT OF PHYSICS

(SUPERVISOR : PROF. DR. ABDULKADIR ŞENOL)

BOLU, JULY 2020

The effects of CP violating dimension-six operators are investigated through $e^+e^- \to H\nu\bar{\nu}$ process in Standard Model Effective Field Theory approach at each energy stages of CLIC with integrated luminosities. Generation of signal and background events are carried out with using Madgraph and passed this generated events through PYTHIA for hadronization and parton showering at parton level. Realistic detector effects are taken into account with using tuned CLIC detector card that is defined in DELPHES. Since in this thesis the Higgs boson are reconstructed from b-jets pair, the limits on CP-violating dimension-six couplings are obtained at three b-tagging working points: tight, medium and loose defined in the CLICdet Card for three energy stages of CLIC (380 GeV, 1.5, 3 TeV). At 3 TeV center of mass energy of CLIC with integrated luminosity of 5 ab^{-1}, on c_{HW} and c_{HB} couplings we had best 95% C.L. limit values which were $|7.0 \times 10^{-3}|$ and $|3.0 \times 10^{-2}|$ for 90% b-tagging efficiency.

KEYWORDS: High energy physics - phenomenology, High energy physics - experiment, Higgs-gauge boson couplings, CP-violating dimension-six operators.

ÖZET

ANORMAL HİGGS-AYAR BOZONU BAĞLAŞIMLARIN HVV ÜRETİM YOLUYLA CLIC'TE İNCELENMESİ
YÜKSEK LİSANS TEZİ
ÖZGÜN KARADENİZ,
BOLU ABANT İZZET BAYSAL UNİVERSİTESİ
LİSANSÜSTÜ EĞİTİM ENSTİTÜSÜ
FİZİK ANABİLİM DALI
(TEZ DANIŞMANI : PROF. DR. ABDULKADİR ŞENOL)
BOLU, TEMMUZ 2020

CP-bozan altı-boyutlu operatörlerin etkileri CLIC'in her bir enerji aşamasında entegre parlaklık değerleriyle birlikte efektif alan teorisi yaklaşımında $e^+e^- \to H\nu\bar{\nu}$ süreci aracılığıyla araştırılmıştır. Madgraph kullanılarak sinyal ve arka alan olaylarının üretimi gerçekleştirilmiş ve üretilen bu olaylar parton seviyesinde, parton sağanağı ve hadronlaştırma için PYTHIA'dan geçirilmiştir. Gerçekçi dedektör etkileri DELPHES içinde tanımlı olan ayarlanmış CLICdet kartı ile dikkate alınmıştır. Bu tezde Higgs bozonu b-jet çiftinden yeniden oluşturulduğu için CP ihlal eden altı-boyutlu bağlaşımların limitleri, CLIC'in üç enerji aşaması için de CLICdet kartında tanımlanan üç b-etiketleme (sıkı, orta, serbest) çalışma noktalarında elde edilmiştir. 95% güvenilirlik seviyesinde en iyi limit değerlerimiz olan $|7.0 \times 10^{-3}|$ and $|3.0 \times 10^{-2}|$, CLIC'in 5 ab^{-1} entegre parlaklık değeri ile 3 TeV kütle merkezi enerjisinde c_{HW} and c_{HB} bağlaşımları üzerinde 90% b-etiketleme verimliliği için elde edilmiştir.

ANAHTAR KELİMELER: Yüksek enerji fiziği - fenomenoloji, Yüksek enerji fiziği - deney, Higgs-ayar bozon bağlaşımları, CP-ihlali 6-boyutlu operatörler.

TABLE OF CONTENTS

LIST OF FIGURES

Page

LIST OF ABBREVIATIONS AND SYMBOLS

ATLAS	: A Toroidal LHC Apparatus.
BEH	: Brout- Englert-Higgs.
BR	: Branching Ratio.
BSM	: Beyond Standard Model.
CERN	: Conseil Europeen pour la recherche nucleaire
CKM	: Cabibbo-Kobayashi-Maskawa.
CLIC	: Compact Linear Collider.
CMS	: Compact Muon Solenoid.
CPV	: CP-Violation.
D-6	:Dimension-six.
EFT	: Effective Field Theory.
EW	: Electro-Weak.
EWSB	: Electro-Weak Symmetry Breaking.
HDO	: Higher-Dimensional Operators.
HE-LHC	: High Energy Large Hadron Collider.
HL-LHC	: High Lumi Large Hadron Collider.
IM	: Invariant Mass.
ISR	: Initial State Radiation.
LHC	: Large Hadron Collider.
MeV	: Mega-Electron Volts.
MC	: Monte Carlo.
NP	: New Physics.
RF	: Radio Frequency.
SSB	: Spontaneous Symmetry Breaking.
SEWSB	: Spontaneous Electro-Weak Symmetry Breaking.
SILH	: Strongly-Interacting Light Higgs.
SM	: Standard Model.
SSB	: Spontaneous Symmetry Breaking.
QCD	: Quantum Chromo Dynamics.
QED	: Quantum Electro Dynamics.
TeV	: Tera-Electron Volts.
VEV	: Vacuum Expectation Value.
WIMP	: Weakly-Interacting Massive Particles.

2HDM	: Two Higgs-Doublet Model.
$\mathbf{p_T}$	: Transverse Momentum.
η	: Pseudo Rapidity.
$\not{E}_\mathbf{T}$	: Missing Transverse Energy.
$\mathbf{H_T}$	: Scalar Transverse Energy Sum.
VLC	: Valencia Linear Collider.
$\tilde{\mathbf{c}}$	: Wilson Coefficient.
$\mathcal{L}$	: Lagrangian.
$\mathcal{O}$	: Operator.
$\chi^\mathbf{2}$	: Chi Square.

ACKNOWLEDGEMENTS

I would like to thank first my advisor Prof.Dr. Abdulkadir Senol who helped me a lot to finish this work. He answered my endless questions about physics patiently and always shared his experience with me not only about physics but also about life. It is not possible to finish this work without his guidance and supports.

I would also thank to Prof.Dr. Haluk Denizli for his precious contributions to my knowledge about physics and supports in projects.

I can not forget the supportive members of our study group. Kaan Yüksel Oyulmaz and Umut Keskin have always been good friends since I joined the group. They had big contributions for this work. I would also express my appreciation to Sinan Öztel and Doğan Avcı. We had very good friendships.

I deeply appreciate to my dear family for being with me in every moment of my life. Especially during in my master education.

I also thank to Scientific and Technological Research Council of Turkey Turkish (TUBITAK) for supporting this thesis work the project under Grant No: 118F333.

I am also thankful to CLICdp working group at CERN for discussions and valuable suggestions in every meeting.

1. INTRODUCTION

Why universe is made by matter? This is a very fundamental question of history of humanity. Nowadays, this very fundamental question is changed with the evolution of physics that why universe is full of matter instead of antimatter? This phenomenon is called baryon asymmetry in the universe by physics society. From some experimental studies (Gorbunov and Rubakov, 2011), it is known that there are much more matter (baryons) than anti-matter (anti-baryons) in the universe.

$$\eta = \frac{\eta_b - \eta_{\bar{b}}}{\eta_\gamma} = \frac{\eta_B}{\eta\gamma} \tag{1.1}$$

where $\eta_B = \eta_b - \eta_{\bar{b}}$ is the density of baryon number. Baryon photon ratio of our universe is found by WMAP experiment which is approximately,

$$\eta \sim 6.1 \times 10^{-10} \tag{1.2}$$

To explain this phenomenon we have three conditions. 1) At Grand Unified Theory scale (10^{16} GeV and 10^{-36} seconds) baryon number violation. 2) CP-violation (CPV) at electroweak (EW) scale (245 GeV and $\leqslant 10^{-12}$) 3) Non-equilibrium evolution of the early universe just after the big-bang. In second case CPV dimension-six (D-6) operator of the Higgs boson couplings with other SM gauge bosons take a key role for spontaneous symmetry breaking (SSB) at EW scale. Although Large Hadron Collider (LHC) provides detailed informations about Standard Model (SM) particles and their interactions but evidence for new physics beyond SM has not been observed in the current experimental results. Many phenomenological studies and give hints about new physics (NP) beyond Standard Model (BSM) to describe CP-violating effects in the Higgs sector (Alloul et al., 2014b; Kumar et al., 2015; Cepeda et al., 2019). As it can be seen from these studies, new upgraded or constructed future colliders are needed. Therefore in this thesis the effects of CPV D-6 operators via $e^+e^- \to \nu\bar{\nu}H$ process was focused in the effective field theory (EFT) framework at the Compact Linear Collider (CLIC) which is planned to construct at CERN.

In Sections 1.1, 1.2, 1.3, 1.4, 1.5, 1.6, 1.7 fundamental knowledges about particle physics and some related topics with the study are introduced. In Chapter 2 the details of EFT approach are given. In chapter 3 briefly mentioned about CLIC and its detector effects. Aim and scope of the study is mentioned in chapter 4. The results of the measurements of three energy stages of CLIC are presented in chapter 5. Finally in chapter 6 all results in the analysis are concluded.

1.1 Standard Model Particles and Interactions

The SM is a theory that classifying elementary particles and describing the interactions between each other via EW and strong forces. To briefly mention about the history of SM, we can go back to 1896 and begin with the discovery of electron by Sir J.J. Thompson in cathode ray tube experiment.

Although the discovery of electron is very important for the SM, 20th century is prime-time of particle physics. In an article, Einstein published in 1905 which gave him nobel prize in 1921, he described photon as "the quanta of light" (Einstein, 1905). Ten years later, Robert Millikan verified in experimentally what Einstein proposed about light (Millikan., 1913). In 1930, Wolfgang Pauli postulated a neutral particle, later called neutrino, based on the conservation of energy in beta decay. In 1956, Clyde Cowan and Frederick Reines detected this spy particle firstly (Cowan et al., 1956). In 1936, while studying cosmic radiation Carl D. Anderson and Seth Neddermeyer proposed a new particle which curved more than proton and less than electron (Neddermeyer and Anderson, 1937). After one year later J. C. Street and E. C. Stevenson confirmed the existence of new particle called muon (Street and Stevenson, 1937). In the middle of 1960s while Murray Gell-Mann and George Zweig were working independently, they proposed the quark model which is a classification of the baryons and mesons using a color symmetry (Gell-Mann, 1957). Almost all of the quarks were discovered during in 1970s, at Stanford Linear Accelerator (up, down, strange, charm) and at Fermilab (bottom) and attracted many Nobel Prizes. With the observation of the top-quark in 1995 at Fermilab (Abachi et al., 1995). All SM particles were accounted for but one; the Higgs boson. Higgs mechanism was developed over 1960s by many physicists including the most important contributions from P. Higgs, R. Brout and F. Englert. They had to wait five decades to see the SM completed by the discovery of the Higgs boson at the LHC in 2012(Aad et al., 2012),(Chatrchyan et al., 2012). SM is a theory that classify particles and describes their interaction between each other (Figure. 1.1). In addition the SM also unifies weak and electromagnetic forces in electroweak (EW) interactions and describing strong interactions with Quantum Chromo Dynamics (QCD). EW interactions and QCD are based on QFT where leptons and quarks are described as fermionic fields which are interact through bosonic fields. The SM separates particles with respect to their spins. Half integer

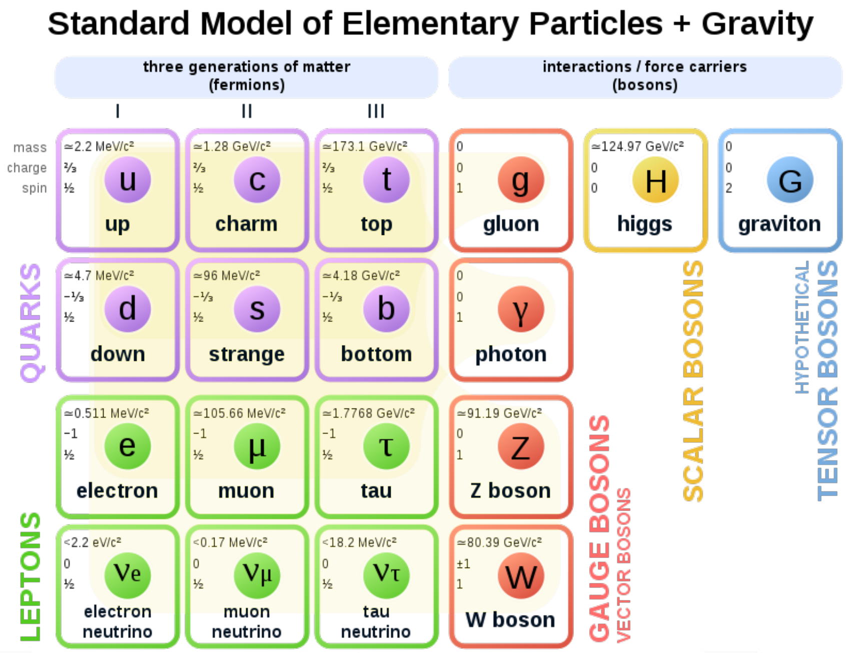

Figure 1.1. SM of particles.

ones are fermions and integer ones are bosons. Opposite quantum numbers and same mass are associated anti-particle.

Fermions: Fermions are elementary particles that their spins are half integer and they are also classified in two group which are called quarks and leptons. In addition they are divided into three families. Every family of quarks contains up and down-type quarks with electric charges are 2/3 and 1/3 respectively. The first family contains stable ones which are ingredients of matter. Further family of quarks are unstable and having higher masses. Leptons are divided two category that are electron-like with charge -1 and neutral neutrinos. First generation of leptons contains an electron and electron-neutrino, second generation have muon and muon-neutrino and third generation contains with tau and tau-neutrino. Electron-like lepton masses are increasing with generation respectively.

Bosons: These particles have integer spin and called force particles. The category contains photons with zero mass, gauge bosons which are $W^{\pm}$, Z^0 and gluons. The boson which generate mass, called Higgs boson with spin 0.

SM consist of three fundamental forces which are electromagnetic, weak and strong. All of these forces have mediators which are associated with vector boson. Electromagnetic force mediates by massless photons and only charged particles can take apart. This means that electromagnetic force can affect all the quarks and fermions.

The strong force is mediated by eight kinds of gluons. They change with respect to their quantum number which is called color. Color charged particles i.e. quarks are affected by strong force.

Z^0 and $W^{\pm}$ bosons are massive vector bosons that are responsible for mediating weak force. Electromagnetic force has long range. In contrast weak and strong forces have short range which is smaller than the size of proton. Furthermore, If strong force is taken one, the EM force is 10^2 times, weak force is 10^5 times and gravitational force is 10^{40} times weaker than strong force. It is not understand why gravitational force is so much weaker than the other force and also this force is currently not part of the SM.

With its particle contents and interactions, the SM is an important theory for understanding the underpinnings of the universe that can explain the phenomenas from the atoms to stars burn. It explains many phenomenons in the universe in very wide range. Nevertheless, the SM has problems to answer some fundamental questions about universe that particle physicists are still trying to shed light on them.

Why Neutrinos have mass?: There are three different types of neutrino which are electron-like, muon-like and tau-like. Although SM predicts that they have no mass, physicists have been found that they can oscillate or transform to another type when they move. This can be possible only when they have mass but after all, the mass of neutrinos are very small. In addition, from some experimental result, there should be a new (fourth) type of neutrino which is called sterile neutrino but so far we have not discovered this spy particles.

Dark Matter: Normally we expect that objects which are near the center of mass, orbit faster than the far ones. In 1968 while Vera Rubin observed the outer stars and near center of mass stars in Andromeda Galaxy, was orbitting same speed. Visible stars masses were not insufficient to hold galaxy together. So there should be an huge amount of matter missing. This missing part is something we can not see which is called "dark matter" that gives additional mass to galaxies. Nowadays many physicists give effort to show the interaction between dark matter and normal matter. In this case we have new models which must be connected the SM.

Why universe is expanding more and more fast?: Hubble space telescope and Gaia measured that universe expansion rate is 45 miles per second per 3.2 million light years with respect to our position. This expansion rate is coming from an unknown feature of the spacetime which is called dark energy.

Gravity: The SM can explain three fundamental forces and their fields except for gravity and its mediator graviton. This force is the weakest force among the other ones about so the any impact of this force on subatomic interactions does not seen.

Why the universe dominated with matter rather than antimatter?: At the beginning of the universe there are equal amount of matter and antimatter. Because of the some reasons which we mentioned at the beginning of the intro, at least around us, universe is dominated by matter.

1.2 CP-Violation

C, P, T operators are very important for particle physics. C operator which is called charge conjugation and responsible for changing particle to its anti-particle. Next, the parity operator P changes spacial vector $P\vec{r} = -\vec{r}$ i.e. mirror image. T operator is responsible for reversing the time axis. In Figure 1.2 P operator provides unphysical decay of π^+ which is $\pi^+ \rightarrow \mu^+ + \nu_\mu$. Because neutrinos are not right-handed fermions. Right handed-fermions means that if the spin and spacial coordinate of particles are in the same direction they are right handed. Otherwise, if they are in opposite direction, they are left-handed fermions. Other operator that of C, provides a decay which is physically allowed.

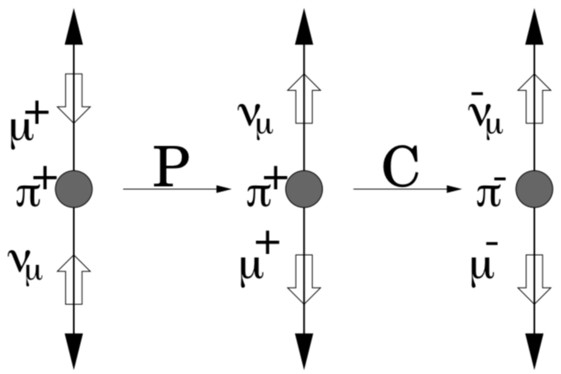

Figure 1.2. P operator transform π^+ decay to forbidden process then C operator changes the situation to physically allowed which is represented in π^- decay. Momentum vectors are represented with solid arrows and the open ones are represents the spin (Tuning, 2020).

Strange implication can be seen on K^0 meson by CP invariance. The second order weak interaction can change K^0 into its antiparticle $\bar{K}^0$. Alternatively, since the K mesons are pseudoscalar, eigenstates of CP can be considered.

$$P|K^0\rangle = -|K^0\rangle, P|\bar{K^0}\rangle = -|\bar{K^0}\rangle \tag{1.3}$$

otherwise,

$$C|K^0\rangle = |\bar{K^0}\rangle, C|\bar{K^0}\rangle = |K^0\rangle \tag{1.4}$$

so under CP,

$$CP|K^0\rangle = -|\bar{K^0}\rangle, CP|\bar{K^0}\rangle = -|K^0\rangle \tag{1.5}$$

Lets define new states

$$|K_1\rangle = \frac{1}{\sqrt{2}}(|K^0\rangle - |\bar{K^0}\rangle) \tag{1.6}$$

under CP

$$CP|K_1\rangle = \frac{1}{\sqrt{2}}(-|K^0\rangle + |\bar{K^0}\rangle) = |K_1\rangle \tag{1.7}$$

which has CP eigenvalue of +1 and a similar calculation for K_2 state

$$|K_2\rangle = \frac{1}{\sqrt{2}}(|K^0\rangle + |\bar{K^0}\rangle) \tag{1.8}$$

$$CP|K_2\rangle = \frac{1}{\sqrt{2}}(-|K^0\rangle - |\bar{K^0}\rangle) = -|K_2\rangle \tag{1.9}$$

which has CP eigenvalue -1. Generally K^0 mesons are decayed into 2π or 3π and each pion has a CP eigenvalue of -1. If we assume that the weak interactions to be invariant under CP transformations, then the CP eigenvalue does not get change during a weak decay.

$$K_1 \rightarrow \pi + \pi, \qquad (+1) \rightarrow (+1) \tag{1.10}$$

and

$$K_2 \rightarrow \pi + \pi + \pi, \qquad (-1) \rightarrow (-1) \tag{1.11}$$

Three pions have approximately the same mass as one kaon, so there is only a small range for the kinetic energy of the resulting pions, which prevents this process to happen often. For a decay into two pions, their kinetic energy can be in a much wider range, rendering this process more probable. For this reason, two types of kaons must be seen in experiments. In 1956, Lederman discovered K_2 meson in his experiment at Brookhaven(Bardon et al., 1958) with two life times.

$$K_S \rightarrow \tau_S = 0.89 \times 10^{-10} sec \qquad K_L \rightarrow \tau_L = 5.2 \times 10^{-8} sec \tag{1.12}$$

As we know that K_1 and K_2 are distinguished by the number of pions, they decay into. Since the decay of K_1 component is faster than K_2, there should be a lot of two pion events near the source. Farther places from the source, the more three pion events are expected to see. It makes sense to identify K_1 with K_S and K_2 with K_L.

$$K_1 = K_S \to \pi + \pi \tag{1.13}$$

$$K_2 = K_L \to \pi + \pi + \pi \tag{1.14}$$

This means that K_S and K_L must have CP eigenstates with the same eigenvalue.

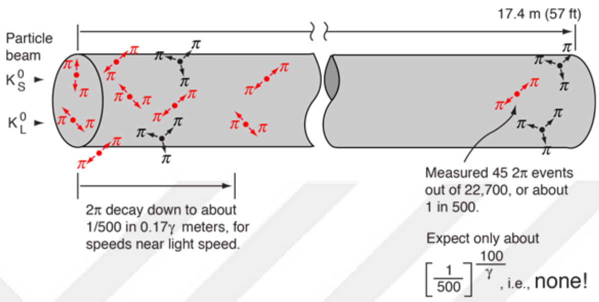

Figure 1.3. Chronin and Fitch experiment with Kaons (LLC, 2018).

In 1964 Cronin and Fitch (Christenson et al., 1964). performed an experiment. They let neutral kaon beams propagate in a long tube. Since the K_L travels much farther than K_S, they arrived arbitrarily pure K_L beam when reaching the detector. The situation that suprised them, they sometimes measured a decay into two pions (Figure 1.3). This means that, a K_L decay into two pions and the CP eigenvalue on the both sides of the equation did not match up.

$$K_L \to \pi + \pi, \qquad (-1) \to (-1)^2 \tag{1.15}$$

We could accept the fact that K_L that is a K_2 can decay weakly not only into three pions, but also into two pions. This would violate CP symmetry in the weak interactions and we call this direct CP violation.

1.3 CKM Matrix

Cabibo-Kobayashi-Maskawa (CKM) (Cabibbo, 1963), (Kobayashi and Maskawa, 1973) is a complex unitary 3×3 matrix which appears in interaction of charged current.

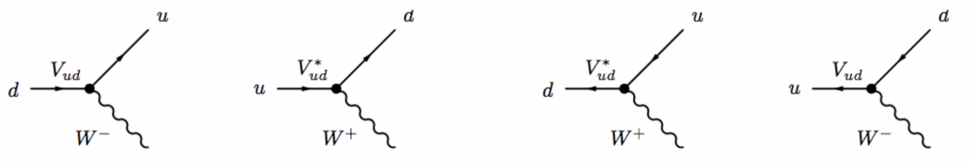

Figure 1.4. Elements and quark mixing of the CKM matrix.

$$V_{CKM} = V_L^u V_L^{u\dagger} = \begin{pmatrix} V_{ud} & V_{us} & V_{ub} \\ V_{cd} & V_{cs} & V_{cb} \\ V_{td} & V_{ts} & V_{ud} \end{pmatrix} \begin{pmatrix} V_{ud}^* & V_{cd}^* & V_{td}^* \\ V_{us}^* & V_{cs}^* & V_{ts}^* \\ V_{ub}^* & V_{cb}^* & V_{tb}^* \end{pmatrix} = \begin{pmatrix} 1 & 0 & 0 \\ 0 & 1 & 0 \\ 0 & 0 & 1 \end{pmatrix} \tag{1.16}$$

Some CKM matrix elements are shown (Figure 1.4). While V_{ud} describes the transition from down quark to up quark, V_{du} describes the transition from top to down quark.The parametrization of CKM matrix is shown in following expression with using three mixing angles,

$$V_{CKM} = \begin{pmatrix} 1 & 0 & 0 \\ 0 & c_{23} & s_{23} \\ 0 & -s_{23} & c_{23} \end{pmatrix} \begin{pmatrix} c_{13} & 0 & s_{13}e^{-i\delta} \\ 0 & 1 & 0 \\ -s_{13}e^{i\delta} & 0 & c_{13} \end{pmatrix} \begin{pmatrix} c_{12} & s_{12} & 0 \\ -s_{12} & c_{12} & 0 \\ 0 & 0 & 1 \end{pmatrix} \tag{1.17}$$

and it becomes the following form,

$$V_{CKM} = \begin{pmatrix} c_{12}c_{13} & s_{12}c_{13} & s_{13}e^{-i\delta} \\ -s_{12}c_{23} - c_{12}s_{23}s_{13}e^{i\delta} & c_{12}c_{23} - s_{12}s_{23}s_{13}e^{i\delta} & s_{23}c_{13} \\ s_{12}s_{23} - c_{12}c_{23}s_{13}e^{i\delta} & -c_{12}s_{23} - s_{12}c_{23}s_{13}e^{i\delta} & c_{23}c_{13} \end{pmatrix} \tag{1.18}$$

where $c_{ij} = \cos\theta_{ij}$, $s_{ij} = \sin\theta_{ij}$ and one phase δ is for CP-violating in flavor changing process in the SM. CKM matrix is parametrized by three mixing angles $\theta_{12}, \theta_{13}, \theta_{23}$ which are between $0°$ and $90°$ so $c_{ij}, s_{ij} \geqslant 0$. CKM angles are important to see deviations from unitary so precision measurement of CKM angles is a good option for finding a sign of new physics. The absolute values for the elements of CKM matrix is given in the following.

$$V_{CKM} = \begin{pmatrix} 0.97427 \pm 0.00014 & 0.22536 \pm 0.00061 & 0.00355 \pm 0.00015 \\ 0.22522 \pm 0.00061 & 0.97343 \pm 0.00015 & 0.0414 \pm 0.0012 \\ 0.00886^{+0.00033}_{-0.00032} & 0.0405^{+0.0011}_{-0.0012} & 0.99914 \pm 0.00005 \end{pmatrix} \tag{1.19}$$

Wolfenstein parametrization is convenient to exhibit this hierarchy. When comparing the Eq. 1.18 and 1.19 we conclude that the $\sin\theta_{ij}$ values are small and that

$\sin\theta_{12} \gg \sin\theta_{23} \gg \sin\theta_{13}$. Then, the Wolfenstein parametrization (Wolfenstein, 1983) define in the following expression,

$$s_{12} = \lambda = \frac{|V_{us}|}{\sqrt{|V_{ud}|^2 + |V_{us}|^2}} \cong 0.22 \tag{1.20}$$

$$s_{23} = A\lambda^2 = \lambda|\frac{V_{cb}}{V_{us}}| \tag{1.21}$$

$$s_{13}e^{i\delta} = V_{ub}^* = A\lambda^3(\rho + i\eta) = \frac{A\lambda^3((\bar{\rho} + i\bar{\eta}))\sqrt{1 - A^2\lambda^4}}{\sqrt{1-\lambda^2}[1 - A^2\lambda^4(\bar{\rho} + i\bar{\eta})]} \tag{1.22}$$

These relations provide that $\bar{\rho} + i\bar{\eta} = -(V_{ud}V_{ub}^*)/(V_{cd}V_{cb}^*)$ is phase convention-independent and the CKM matrix can be written with λ, A, $\bar{\rho}$ and $\bar{\eta}$ parameters can reproduce the results. For instance, $\bar{\rho} = \rho(1 - \lambda^2/2 + ...)$ so we can write the CKM matrix in the following form,

$$V_{CKM} = \begin{pmatrix} 1 - \lambda^2/2 & \lambda & A\lambda^3(\rho - i\eta) \\ -\lambda & 1 - \lambda^2/2 & A\lambda^2 \\ A\lambda^3(1 - \rho - i\eta) & -A\lambda^2 & 1 \end{pmatrix} \tag{1.23}$$

A, ρ and η parameters are used for unitary. In addition, from unitary relation we know that $V^\dagger V = 1$. From this, we get some orthogonality conditions. The expressions in below is related with the complex phase. In fact, they are compilation of three complex numbers that the results must be zero. So it can be said that they are like a triangle in the complex plane.

$$V_{ud}V_{cd}^* + V_{us}V_{cs}^* + V_{ub}V_{cb}^* = 0 \tag{1.24}$$

$$V_{ud}V_{td}^* + V_{us}V_{ts}^* + V_{ub}V_{tv}^* = 0 \tag{1.25}$$

$$V_{cd}V_{ud}^* + V_{cs}V_{us}^* + V_{cb}V_{ub}^* = 0 \tag{1.26}$$

$$V_{cd}V_{td}^* + V_{cs}V_{ts}^* + V_{cb}V_{tb}^* = 0 \tag{1.27}$$

$$V_{td}V_{ud}^* + V_{ts}V_{cs}^* + V_{tb}V_{ub}^* = 0 \tag{1.28}$$

$$V_{td}V_{cd}^* + V_{ts}V_{cs}^* + V_{tb}V_{cb}^* = 0 \tag{1.29}$$

Here we considered two equations from these orthogonalities which contained λ with same power $\mathcal{O}(\lambda^3)$.

$$V_{ud}V_{ub}^* + V_{cd}V_{cb}^* + V_{td}V_{tb}^* = 0, V_{td}V_{ud}^* + V_{ts}V_{us}^* + V_{tb}V_{ub}^* = 0 \tag{1.30}$$

By dividing each side of the first expression in Eq. 1.30 with $|V_{cd}V_{cb}|$ and then rotating the triangle, it gives the well known unitary triangle which is shown (Figure 1.5).

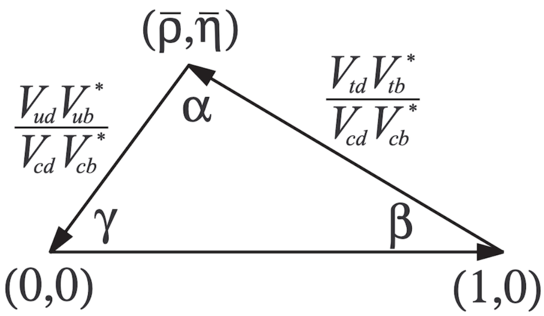

Figure 1.5. Illustration of the unitary triangle.

α, β and γ angles define in the following:

$$\alpha \equiv \arg[-\frac{V_{td}V_{tb}^*}{V_{ud}V_{ub}^*}], \beta \equiv \arg[-\frac{V_{cd}V_{cb}^*}{V_{td}V_{tb}^*}], \gamma \equiv \arg[-\frac{V_{ud}V_{ub}^*}{V_{cd}V_{cb}^*}] \tag{1.31}$$

For observing CP violation it is required to be $V_{ij} \neq V_{ij}^*$. This is valid if finite surface of triangle is in the complex plane. The surface area of all unitary triangles are same. This number is denoted with J which is called Jarlskog invariant. It is a phase-convention-independent measure of CPV and defined by $Im[V_{ij}V_{kl}V_{il}^*V_{kj}^*] = J\sum_{m,n}\epsilon_{ikm}\epsilon_{jln}$. From Eq. 1.18 Jarlskof invariant is

$$J = c_{12}c_{12}^2c_{23}s_{12}s_{13}s_{23}\sin\delta_{13} \tag{1.32}$$

This expressions occurs in all CPV effects. If the value of one mixing angle is zero, the value of J is zero. In other words, there is no possible CPV, the complex phase will be zero. Finally the value of J is equal to the two times of the unitary triangle surface area. For new physics searches it is necessary to investigate the angles of triangle. If there is a conflict between lengths and angles, it is pointed out a new physics. (Ceccucci et al., 2018)

1.4 Electroweak Interactions

At the end of the 1970's three famous physicist won the Nobel Prize for their work that was the unification of the weak and electromagnetic forces.The weak interactions are the only interactions that are directly responsible for particle decays. Unlike the electromagnetic and strong interactions, every SM particles feel the weak interactions. For example neutrinos do not feel the electromagnetic interactions because the do not carry electric charge. They only feel weak interactions. Moreover, lepton do not feel strong interactions because they do not have color charge. However, every single particle regardless whether they have color and electromagnetic charge , they feel the electroweak interactions. In addition weak interactions violate C, P, CP and T discrete symmetries.

The weak interactions themselves are not based on symmetry that we observed in nature. They are actually based on symmetry that is broken. For the unification of the weak and electromagnetic interactions, global symmetries which $SU(2)_L \times U(1)_Y$ fit onto local interactions. These two groups together, form the electroweak interactions. Here Y is called hypercharge and it is different from electromagnetic charge. L is called left chirality of a spinnor, it is related to parity violation which is mentioned in Sec. 1.2. The left handed doublets are shown in the following.

$$\begin{pmatrix} \nu_e \\ e \end{pmatrix}, \begin{pmatrix} \nu_\mu \\ \mu \end{pmatrix}, \begin{pmatrix} \nu_\tau \\ \tau \end{pmatrix}, \begin{pmatrix} u \\ d \end{pmatrix}_L, \begin{pmatrix} c \\ s \end{pmatrix}_L, \begin{pmatrix} t \\ b \end{pmatrix}_L$$

$SU(2)_L$ matrix can act on these left handed doublets and convert it another flavor.

$$\begin{pmatrix} 1 \\ 0 \end{pmatrix} \xrightarrow{SU(2)_L} \begin{pmatrix} 0 \\ 1 \end{pmatrix} \tag{1.33}$$

This is a simple example of the nature of flavor change in the weak interactions.

$$e_R, \mu_R, \tau_R, u_R, d_R, c_R, s_R, t_R, b_R$$

Since there are three Pauli matrices, $SU(2)_L$ has three generators where $T_a = \frac{1}{2}\sigma_a$. σ is Pauli matrix. We have new form of the wave function with applying local gauge transformation.

$$\psi(x) \to \psi'(x) = e^{i\theta^a(x)T_a}\psi(x), a = 1, 2, 3 \tag{1.34}$$

We need three gauge field in order to have invariance Lagrangian,

$$W^a_\mu(x) \to W'^a_\mu(x) = W^a_\mu(x) + \frac{1}{g}\partial_\mu \theta^a(x) + \epsilon^{abc}W^b_\mu(x)\theta^c(x), a = 1, 2, 3 \tag{1.35}$$

Here g is coupling constant and ϵ is structure constant. Next we must define covariant derivative.

$$\partial_\mu \to D_\mu = \partial_\mu - igT_a W^a_\mu(x) \tag{1.36}$$

It is necessary to add kinetic term in order to allow the propagation of fields,

$$\mathcal{L} = -\frac{1}{4}W^a_{\mu\nu}W^{\mu\nu}_a \tag{1.37}$$

where $W^a_{\mu\nu}$ is a field tensor and the expression is,

$$W^a_{\mu\nu} = \partial_\mu W^a_\nu - \partial_\nu W^a_\mu \tag{1.38}$$

So far we have four new gauge fields, three for $SU(2)_L$ (W^1, W^2, W^3) and one for $U(1)_Y(A_\mu)$. Covariant derivative must be defined for unified theory which $SU(2)_L \times U(1)_Y$ local gauge symmetry acts on.

$$D^{L,R}_\mu = \partial_\mu - igI^{L,R}_a W^a_\mu - i\frac{g'}{2} Y B_\mu, I^L_a = \frac{1}{2}\sigma_a, I^R_a = 0 \tag{1.39}$$

The last term of the Eqn. 1.39, we do not need left component because $SU(2)_L$ does not act on right component. The following expression represents charged weak bosons with using the combination of first and second component of $SU(2)_L$.

$$W^{\pm\mu} = \frac{W^\mu_1 + W^\mu_2}{\sqrt{2}} \tag{1.40}$$

These gauge bosons take a role for particle decays. For example,

$$W^+_\mu = \begin{pmatrix} 0 & 1 \\ 0 & 0 \end{pmatrix}, e^- = \begin{pmatrix} 0 \\ 1 \end{pmatrix}, \begin{pmatrix} 1 \\ 0 \end{pmatrix} \Longrightarrow \begin{pmatrix} 0 \\ 1 \end{pmatrix} \begin{pmatrix} 0 & 1 \\ 0 & 0 \end{pmatrix} = \begin{pmatrix} 1 \\ 0 \end{pmatrix}$$

And the representation of photon and Z boson is the combination of B_μ, is the unique component of $U(1)_Y$ and W^3 which is the third component of $SU(2)_L$

$$A_\mu = B_\mu \cos\theta_w + W^3 \sin\theta_w,\ Z_\mu = -B_\mu \sin\theta_w + W^3 \cos\theta_w \tag{1.41}$$

A_μ is the boson that is called photon of EM and Z is neutral boson of the weak interactions.

1.5 Spontaneously Electroweak Symmetry Breaking

First of all lets define a new scalar field.

$$\phi = \frac{1}{2}(\phi_1 + i\phi_2) \tag{1.42}$$

Lagrangian which contains informations about the way the field behaves.

$$\mathcal{L} = (D^\mu\phi)^\dagger(D_\mu\phi) - V(\phi) - \frac{1}{4}F_{\mu\nu}F^{\mu\nu}. \tag{1.43}$$

Where $V(\phi) = \mu^2(\phi^\dagger\phi) + \lambda(\phi^\dagger\phi)^2$ and $\lambda > 0$, $\mu^2 < 0$, $D_{mu} = \partial_\mu - ieA_\mu(x)$.
From the equation it can be seen that the Lagrangian is symmetric because all the powers of

field are even ($\mathcal{L}(\phi) = \mathcal{L}(-\phi)$). Here μ is related with the mass of any excited particle of the field.

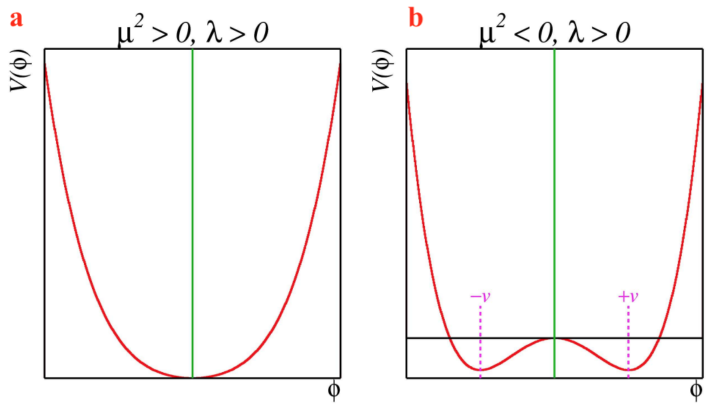

Figure 1.6. Higgs potential respect to sign of μ^2.

λ is dimensionless coupling constant in the quartic part and it is a kind of self interaction. To find the effects of this new scalar field on the Lagrangian, it is necessary to find the minimum potential which called vacuum. Mathematically $\partial V(\phi)/\partial\phi = 0$ relation tells, vacuum which is the lowest potential energy that corresponds to $\phi(0) \neq 0$ and it takes the value of $\pm\nu$ (Figure 1.6). This relation gives rise to circle of vacua $\sqrt{\frac{-\mu^2}{2\lambda}}$ and it breaks the symmetry of Lagrangian. A common expression for the vacuum shown in follow.

$$\phi_{1,vac} = \sqrt{\frac{-\mu^2}{2\lambda}} \equiv \frac{\nu}{\sqrt{2}}, \quad \phi_{2,vac} = 0. \tag{1.44}$$

Here ν is called vacuum expectation value (VEV). The following equation is the transformation of ϕ to keep the Lagrangian invariant,

$$\phi(x) \rightarrow \phi'(x) = e^{-i\alpha(x)} \tag{1.45}$$

With adding small shift the new scalar field becomes,

$$\phi = \frac{1}{2}(\eta + \nu + i\zeta) \tag{1.46}$$

after this perturbation the Lagrangian form is changed as in below,

$$\mathcal{L}(\eta,\zeta) = \frac{1}{2}(\partial_\mu\eta)^2 - \lambda\nu^2\eta^2 + \frac{1}{2}(\partial_\mu\zeta)^2 - \frac{1}{4}F_{\mu\nu}F^{\mu\nu} + \frac{1}{2}e^2\nu^2A_\mu^2 - eA_\mu\nu(\partial^\mu\zeta) + int.terms. \tag{1.47}$$

where the first and the second terms is about η-particle, the third term is about ζ, the fourth term and the fifth terms are for photon field. In this Lagrangian η-particle is a massive particle with mass of $\sqrt{-\mu^2}$ and ζ-particle is massless which is called Goldstone boson. To get a real scalar field, the local phase transformation can be applied,

$$.\phi \to \phi' = e^{-i\zeta(x)/\nu}\phi = \frac{\nu + \eta}{\sqrt{2}}. \tag{1.48}$$

Next replace η with h which is real scalar Higgs field,

$$\phi' = \frac{\nu + h}{\sqrt{2}}. \tag{1.49}$$

After, the Lagrangian for becomes,

$$\mathcal{L}_{scalar} = \frac{1}{2}(\partial_\mu h)^2 - \lambda\nu^2 h^2 - \frac{1}{2}e^2\nu^2 A_\mu^2 + \frac{1}{4}F_{\mu\nu}F^{\mu\nu} + e^2\nu A_\mu^2 + \frac{1}{2}e^2 A_\mu^2 h^2 - \lambda\nu h^3 - \frac{1}{4}\lambda h^4 \tag{1.50}$$

First term is about E_{kin} and and the mass term of Higgs, second term is for mass term of the gauge boson and E_{kin}, third terms represents the interaction of the Higgs and gauge field ($A_\mu^2 h^2$) and the last term express the Higgs field self interaction.

In summary, when complex scalar field corresponds to ν it yields to break the symmetry. This provides the generation for mass of gauge boson. In addition real scalar gauge boson with mass that can be called the Higgs boson.

1.6 The Higgs Mechanism

Here the unified EW theory ($SU(2)_L \times U(1)_L$) are not taken into account because that is not what we observe in the experiments. We observe electromagnetic and broken weak interactions which mentioned in the previous section. Higgs mechanism in the SM, provides three massive gauge bosons $W^{\pm}$, Z^0 while leaving photon massless. In addition it generates mass for fermions. Different from previous section a unique Higgs doublet is defined,

$$\phi = \begin{pmatrix} \phi^+ \\ \phi^0 \end{pmatrix} = \frac{1}{\sqrt{2}} \begin{pmatrix} \phi_1 + i\phi_2 \\ \phi_3 + i\phi_4 \end{pmatrix} \tag{1.51}$$

The Lagrangian for this doublet is

$$\mathcal{L}_{scalar} = (D^\mu\phi)^\dagger(D_\mu\phi) - V(\phi) \tag{1.52}$$

Where $V(\phi) = \mu^2(\phi^\dagger\phi) + \lambda(\phi^\dagger\phi)^2$ with $\mu^2 < 0$, and

$$D_\mu = \partial_\mu + ig\frac{1}{2}\overrightarrow{\tau}.\overrightarrow{W_\mu} + ig'\frac{1}{2}YB_\mu \tag{1.53}$$

The theory contains just left handed doublet with $I = \frac{1}{2}$. As we have seen in the previous case, for$\mu^2 < 0$, the potential would have infinite number of vacua, so it does not preserve the symmetry of the Lagrangian. A convenient choice for a physical vacuum state would be $\phi_1 = \phi_2 = \phi_4 = 0$ and $\phi_3 = \frac{\nu}{\sqrt{2}}$ so the vacuum can be defined as,

$$\phi_0 = \begin{pmatrix} 0 \\ \nu/\sqrt{2} \end{pmatrix} \tag{1.54}$$

Lets redefine 1.52 with rewriting by h which is scalar Higgs field. Also with expressing covariant derivative in the following,

$$D_\mu \phi = \partial_\mu + ig\frac{1}{2}\overrightarrow{\tau}.\overrightarrow{W_\mu} + ig'\frac{1}{2}YB_\mu \begin{pmatrix} 0 \\ \nu + \nu/\sqrt{2} \end{pmatrix} \tag{1.55}$$

In order to focus on mass term only ν^2 parts are taken to account in Eq.1.50.

$$(D^\mu\phi)^\dagger(D_\mu\phi) = (-i\frac{g}{2}(\tau_1 W_1 + \tau_2 W_2 + \tau_3 W_3) - i\frac{g'}{2}B_\mu \begin{pmatrix} 0 \\ \nu/\sqrt{2} \end{pmatrix})^2 \tag{1.56}$$

W_1 and W_2 are substittued with $W^\pm$ with respect to Eq.1.40 and Eq.1.56 in the following for,

$$(D^\mu\phi)^\dagger(D_\mu\phi) = ((\frac{1}{2}\nu g)^2 W_\mu^+ W^{-\mu} + \frac{1}{8}\nu^2(W_\mu^3, B_\mu) \begin{pmatrix} g^2 & -gg' \\ -gg' & g'^2 \end{pmatrix} \begin{pmatrix} W^{3\mu} \\ B^\mu \end{pmatrix})^2 \tag{1.57}$$

Here $W^\pm$ is the force mediator of electroweak interactions and the mass term is in the following,

$$m_w = \frac{1}{2}g\nu \tag{1.58}$$

In addition A_μ and Z_μ fields are corresponding to γ and Z boson which are obtained from the combination of W_3 and B_μ shown in Eq.1.41. With matrix below these two gauge bosons mass can be computed,

$$M = \begin{pmatrix} g^2 & -gg' \\ -gg' & g'^2 \end{pmatrix} \tag{1.59}$$

The eigenvalues of this matrix are λ = 0 and λ = $(g^2 + g'^2)$. the eigenvalue of A_μ is zero so the mass of photon field is zero. In addition the eigenvalue of Z-boson,

$$Z_\mu = \frac{1}{\sqrt{g^2 + g'^2}}(gW_3 + g'B_\mu) \tag{1.60}$$

with mass $m_z = \frac{1}{2}\nu\sqrt{g^2 + g'^2}$. With non-vanishing VEV, the consequence of broken symmetry of global $SU(2)_L \times U(1)_Y$ group, massive $W^\pm$ and Z^0 bosons are obtained and photon remains massless. Also generate the Higgs boson which is a massive scalar particle.

1.7 The Higgs Boson Beyond Standard Model

Although SM is a coherent model to describe the particle and their interactions, it is insufficient to explain some of the phenomena in the universe. One of the problem about explaining among the phenomenons, is CPV in the Higgs sector. This can be explain the matter-antimatter asymmetry in the universe. The effect of CPV in SM, is very small so this asymmetry can not observe in SM framework. It is necessary to extend the theory beyond the SM.

There are some models which Minimal Composite Higgs Model that is about the light Higgs. Another model which is incorporate with CPV, is Two Higgs Doublet Model (Branco et al., 2012).

2. THEORETICAL FRAMEWORK

It is well known that the Quantum Field Theory QFT is a theory that describes elementary particles and their interactions based on SM gauge symmetry $SU(3)_c \times SU(2)_L \times U(1)_Y$. In detail the first group $SU(3)_c$ defines strong interactions with its particles gluons and c represents color. $SU(2)_L \times U(1)_Y$ part of the gauge group is related with weak and EM interactions with its particles $W^{\pm}$, Z^0 and γ after EWSB. L subscript represents left-handedness and Y for hyperchange. This expression basically contains all elementary particles which are observed up to this time, and their interactions only except gravity particle graviton. In Eq.2.1 notations and adjoint representations of the gauge subgroups are given.

$$SU(3)_c \to G^a_\mu = (\tilde{\mathbf{8}}, \tilde{\mathbf{1}}, 0)\ , \quad SU(2)_L \to W^k_\mu = (\tilde{\mathbf{1}}, \tilde{\mathbf{3}}, 0)\ , \quad U(1)_Y \to B_\mu = (\tilde{\mathbf{1}}, \tilde{\mathbf{1}}, 0)\ , \tag{2.1}$$

Gauge boson dynamics also define with strength tensors field in Lagrangian.

$$\mathcal{L}_{\text{gauge}} = -\frac{1}{4} G^a_{\mu\nu} G^{\mu\nu}_a - \frac{1}{4} W^a_{\mu\nu} W^{\mu\nu}_a - \frac{1}{4} B^a_{\mu\nu} B^{\mu\nu}_a . \tag{2.2}$$

For $SU(3)_c$ the strength tensor field labeled as G, W for $SU(2)_L$ and B for $SU(1)_Y$. The expansion of these fields will given in Section 2.1, The chiral content of the theory is defined by three generations of left-handed and right-handed quark (Q_L, u_R and d_R) and lepton (L_L and e_R) fields.

$$\begin{aligned} Q_L &= \begin{pmatrix} u_L \\ d_L \end{pmatrix} = (\tilde{\mathbf{3}}, \tilde{\mathbf{2}}, \frac{1}{6})\ , \quad u_R = (\tilde{\mathbf{3}}, \tilde{\mathbf{1}}, \frac{2}{3})\ , \quad d_R = (\tilde{\mathbf{3}}, \tilde{\mathbf{1}}, -\frac{1}{3})\ , \\ L_L &= \begin{pmatrix} \nu_L \\ \ell_L \end{pmatrix} = (\tilde{\mathbf{1}}, \tilde{\mathbf{2}}, -\frac{1}{2})\ , \quad e_R = (\tilde{\mathbf{1}}, \tilde{\mathbf{1}}, -1)\ , xs \end{aligned} \tag{2.3}$$

Finally, the Higgs sector contains a single $SU(2)_L$ doublet of fields, which causes SSB via $Higgs\ mechanism$.

$$\Phi = \begin{pmatrix} -iG^+ \\ \frac{1}{\sqrt{2}}\left[v + h + iG^0\right] \end{pmatrix} = (\tilde{\mathbf{1}}, \tilde{\mathbf{2}}, \frac{1}{2})\ . \tag{2.4}$$

2.1 Effective Field Theory

EFT approach is a quite good option for parametrizing deviations from SM. In this thesis, 59 independent 6-D operators are employed and 5-D operators which are related with Majorana neutrinos and 8-D operators' effects are neglected. In this EFT, SM and relevant Lagrangians are used which extended with higher-dimensional-operators (HDO) coefficients.

$$\mathcal{L}_{\text{eff}} = \mathcal{L}_{\text{SM}} + \sum_i \frac{c_i}{\Lambda^2}\mathcal{O}_i \ . \tag{2.5}$$

here Λ is inverse power of mass and represents new physics scale. $\mathcal{O}$ is HDO basis which composed of the SM fields are restricted by the symmetry groups. In other words, Higgs doublets, gauge bosons, fermionic fields and derivative of this fields. New physics (NP) couplings' dimensionless parameters are represented by the coefficient c_i. EFT provides to characterize the features of the newly discovered Higgs boson, and has some positive advantages such as renormalizable in the expansion of E/Λ respectively. Here E is an energy for the related process. EFT has largely studied for Higgs sector, although it has disadvantages something like the loss of unitary which is because of E greater than Λ. The theory is also a good method to study in the limit of low energy scale which is about W boson mass m_W or VEV of the Higgs field v. Mainly writing out the convenient set of Lagrangians with respect to theories of symmetries. In these energy scale and VEV, in the EFT approach that we consider, SM Lagrangian is supported by HDO that determine the effects of unobserved conditions.

$$\mathcal{L}_{\text{eff}} = \mathcal{L}_{\text{SM}} + \sum_i \bar{c}_i\mathcal{O}_i = \mathcal{L}_{\text{SM}} + \mathcal{L}_{\text{SILH}} + \mathcal{L}_{CP} + \mathcal{L}_{F_1} + \mathcal{L}_{F_2} + \mathcal{L}_G \ , \tag{2.6}$$

The first terms of this expansion, $\mathcal{L}_{\text{SILH}}$, has the operators of CP-conserving with the Higgs doublet Φ. (Alloul et al., 2014b)

$$\begin{aligned}\mathcal{L}_{\text{SILH}} = {} & \frac{\bar{c}_H}{2v^2}\partial^\mu\big[\Phi^\dagger\Phi\big]\partial_\mu\big[\Phi^\dagger\Phi\big] + \frac{\bar{c}_T}{2v^2}\big[\Phi^\dagger\overleftrightarrow{D}^\mu\Phi\big]\big[\Phi^\dagger\overleftrightarrow{D}_\mu\Phi\big] - \frac{\bar{c}_6\lambda}{v^2}\big[\Phi^\dagger\Phi\big]^3 \\ & - \left[\frac{\bar{c}_u}{v^2}y_u\Phi^\dagger\Phi\ \Phi^\dagger\cdot\bar{Q}_L u_R + \frac{\bar{c}_d}{v^2}y_d\Phi^\dagger\Phi\ \Phi\bar{Q}_L d_R + \frac{\bar{c}_l}{v^2}y_\ell\ \Phi^\dagger\Phi\ \Phi\bar{L}_L e_R + \text{h.c.}\right] \\ & + \frac{ig\ \bar{c}_W}{m_W^2}\big[\Phi^\dagger T_{2k}\overleftrightarrow{D}^\mu\Phi\big]D^\nu W^k_{\mu\nu} + \frac{ig'\ \bar{c}_B}{2m_W^2}\big[\Phi^\dagger\overleftrightarrow{D}^\mu\Phi\big]\partial^\nu B_{\mu\nu} \\ & + \frac{2ig\ \bar{c}_{HW}}{m_W^2}\big[D^\mu\Phi^\dagger T_{2k}D^\nu\Phi\big]W^k_{\mu\nu} + \frac{ig'\ \bar{c}_{HB}}{m_W^2}\big[D^\mu\Phi^\dagger D^\nu\Phi\big]B_{\mu\nu} \\ & + \frac{g'^2\ \bar{c}_\gamma}{m_W^2}\Phi^\dagger\Phi B_{\mu\nu}B^{\mu\nu} + \frac{g_s^2\ \bar{c}_g}{m_W^2}\Phi^\dagger\Phi G^a_{\mu\nu}G_a^{\mu\nu}\ ,\end{aligned} \tag{2.7}$$

here, λ represents the quartic couplings of Higgs. In flavour space y_u, y_d and y_ℓ are 3×3 Yukawa matrices. In this equation, g', g and g_s are the coupling constants of $U(1)_Y$, $SU(2)_L$

and $SU(3)_c$ respectively while $T_{2k} = \sigma_k/2$, σ_k is $SU(2)_L$ generators which is given in fundamental representation. Representation of derivative of Hermitian operator is given by Eq. 2.8

$$\Phi^\dagger \overleftrightarrow{D}_\mu \Phi = \Phi^\dagger D^\mu \Phi - D_\mu \Phi^\dagger \Phi \ , \tag{2.8}$$

In following expressions, tensors of field-strength and the derivatives of gauge-covariant are represented.

$$\begin{aligned}
B_{\mu\nu} &= \partial_\mu B_\nu - \partial_\nu B_\mu \ , \\
W^k_{\mu\nu} &= \partial_\mu W^k_\nu - \partial_\nu W^k_\mu + g\epsilon_{ij}{}^k\, W^i_\mu W^j_\nu \ , \\
G^a_{\mu\nu} &= \partial_\mu G^a_\nu - \partial_\nu G^a_\mu + g_s f_{bc}{}^a\, G^b_\mu G^c_\nu \ , \\
D_\rho W^k_{\mu\nu} &= \partial_\mu \partial_\rho W^k_\nu - \partial_\nu \partial_\rho W^k_\mu + g\epsilon_{ij}{}^k \partial_\rho \big[W^i_\mu W^j_\nu\big] + g\epsilon_{ij}{}^k W^i_\rho \big[\partial_\mu W^j_\nu - \partial_\nu W^j_\mu\big] \\
&\quad + g^2 W_{\rho i}\big[W^i_\nu W^k_\mu - W^i_\mu W^k_\nu\big] \ , \\
D_\mu \Phi &= \partial_\mu \Phi - \frac{1}{2} i g' B_\mu \Phi - i g T_{2k} W^k_\mu \Phi \ ,
\end{aligned} \tag{2.9}$$

The third term in Eq. 2.6, $\mathcal{L}_{CP}$, will discuss in Section 2.2 . Next the fourth term in Eq. 2.6 $\mathcal{L}_{F_1}$, defines the interactions between quarks, lepton pairs and two Higgs fields.

$$\begin{aligned}
\mathcal{L}_{F_1} = & \frac{i\bar{c}_{HQ}}{v^2}\big[\bar{Q}_L \gamma^\mu Q_L\big]\big[\Phi^\dagger \overleftrightarrow{D}_\mu \Phi\big] + \frac{4i\bar{c}'_{HQ}}{v^2}\big[\bar{Q}_L \gamma^\mu T_{2k} Q_L\big]\big[\Phi^\dagger T^k_2 \overleftrightarrow{D}_\mu \Phi\big] \\
& + \frac{i\bar{c}_{Hu}}{v^2}\big[\bar{u}_R \gamma^\mu u_R\big]\big[\Phi^\dagger \overleftrightarrow{D}_\mu \Phi\big] + \frac{i\bar{c}_{Hd}}{v^2}\big[\bar{d}_R \gamma^\mu d_R\big]\big[\Phi^\dagger \overleftrightarrow{D}_\mu \Phi\big] \\
& - \left[\frac{i\bar{c}_{Hud}}{v^2}\big[\bar{u}_R \gamma^\mu d_R\big]\big[\Phi \cdot \overleftrightarrow{D}_\mu \Phi\big] + \text{h.c.}\right] \\
& + \frac{i\bar{c}_{HL}}{v^2}\big[\bar{L}_L \gamma^\mu L_L\big]\big[\Phi^\dagger \overleftrightarrow{D}_\mu \Phi\big] + \frac{4i\bar{c}'_{HL}}{v^2}\big[\bar{L}_L \gamma^\mu T_{2k} L_L\big]\big[\Phi^\dagger T^k_2 \overleftrightarrow{D}_\mu \Phi\big] \\
& + \frac{i\bar{c}_{He}}{v^2}\big[\bar{e}_R \gamma^\mu e_R\big]\big[\Phi^\dagger \overleftrightarrow{D}_\mu \Phi\big] \ ,
\end{aligned} \tag{2.10}$$

The fifth term in Eq. 2.6, $\mathcal{L}_{F_2}$, represents the interactions between one single Higgs fields, gauge boson and lepton or quark.

$$\begin{aligned}
\mathcal{L}_{F_2} = \Bigg[& -\frac{2g'\,\bar{c}_{uB}}{m^2_W} y_u\, \Phi^\dagger \cdot \bar{Q}_L \gamma^{\mu\nu} u_R\, B_{\mu\nu} - \frac{4g\,\bar{c}_{uW}}{m^2_W} y_u\, \Phi^\dagger \cdot \big(\bar{Q}_L T_{2k}\big)\gamma^{\mu\nu} u_R\, W^k_{\mu\nu} \\
& - \frac{4g_s\,\bar{c}_{uG}}{m^2_W} y_u\, \Phi^\dagger \cdot \bar{Q}_L \gamma^{\mu\nu} T_a u_R G^a_{\mu\nu} + \frac{2g'\,\bar{c}_{dB}}{m^2_W} y_d\, \Phi \bar{Q}_L \gamma^{\mu\nu} d_R\, B_{\mu\nu} \\
& + \frac{4g\,\bar{c}_{dW}}{m^2_W} y_d\, \Phi\big(\bar{Q}_L T_{2k}\big)\gamma^{\mu\nu} d_R\, W^k_{\mu\nu} + \frac{4g_s\,\bar{c}_{dG}}{m^2_W} y_d\, \Phi \bar{Q}_L \gamma^{\mu\nu} T_a d_R G^a_{\mu\nu} \\
& + \frac{2g'\,\bar{c}_{eB}}{m^2_W} y_\ell\, \Phi \bar{L}_L \gamma^{\mu\nu} e_R\, B_{\mu\nu} + \frac{4g\,\bar{c}_{eW}}{m^2_W} y_\ell\, \Phi\big(\bar{L}_L T_{2k}\big)\gamma^{\mu\nu} e_R\, W^k_{\mu\nu} + \text{h.c.}\Bigg] \ .
\end{aligned} \tag{2.11}$$

The last term in Eq. 2.6, $\mathcal{L}_G$, is not directly about Higgs, it is about the gauge boson self interactions.

$$\mathcal{L}_G = \frac{g^3\, \bar{c}_{3W}}{m_W^2}\epsilon_{ijk}W^i_{\mu\nu}W^{\nu j}_{\ \rho}W^{\rho\mu k} + \frac{g_s^3\, \bar{c}_{3G}}{m_W^2} f_{abc}G^a_{\mu\nu}G^{\nu b}_{\ \rho}G^{\rho\mu c} + \frac{\bar{c}_{2W}}{m_W^2}D^\mu W^k_{\mu\nu}D_\rho W^{\rho\nu}_k + \frac{\bar{c}_{2B}}{m_W^2}\partial^\mu B_{\mu\nu}\partial_\rho B^{\rho\nu} + \frac{\bar{c}_{2G}}{m_W^2}D^\mu G^a_{\mu\nu}D_\rho G^{\rho\nu}_a \ , \tag{2.12}$$

with

$$D_\rho G^a_{\mu\nu} = \partial_\mu\partial_\rho G^a_\nu - \partial_\nu\partial_\rho G^a_\mu + g_s f_{bc}{}^a \partial_\rho\big[G^b_\mu G^c_\nu\big] + g_s f_{bc}{}^a G^b_\rho\big[\partial_\mu G^c_\nu - \partial_\nu G^c_\mu\big] + g_s^2 G_{\rho b}\big[G^b_\nu G^a_\mu - G^b_\mu G^a_\nu\big] \ , \tag{2.13}$$

2.2 Effective CP-Violating Lagrangian

The D-6 CPV interaction of Higgs boson and electroweak gauge boson in the SILH bases given in the folllowing equation. (The third term of the Eq. 2.6 contains CPV operators)

$$\mathcal{L}_{CP} = \frac{ig\, \tilde{c}_{HW}}{m_W^2}D^\mu\Phi^\dagger T_{2k}D^\nu\Phi\widetilde{W}^k_{\mu\nu} + \frac{ig'\, \tilde{c}_{HB}}{m_W^2}D^\mu\Phi^\dagger D^\nu\Phi\widetilde{B}_{\mu\nu} + \frac{g'^2\, \tilde{c}_\gamma}{m_W^2}\Phi^\dagger\Phi B_{\mu\nu}\widetilde{B}^{\mu\nu} + \frac{g_s^2\, \tilde{c}_g}{m_W^2}\Phi^\dagger\Phi G^a_{\mu\nu}\widetilde{G}^{\mu\nu}_a + \frac{g^3\, \tilde{c}_{3W}}{m_W^2}\epsilon_{ijk}W^i_{\mu\nu}W^{\nu j}_{\ \rho}\widetilde{W}^{\rho\mu k} + \frac{g_s^3\, \tilde{c}_{3G}}{m_W^2}f_{abc}G^a_{\mu\nu}G^{\nu b}_{\ \rho}\widetilde{G}^{\rho\mu c} \ , \tag{2.14}$$

the expressions of dual strength tensors of of W-boson, Z-boson and photon are in below,

$$\widetilde{B}_{\mu\nu} = \frac{1}{2}\epsilon_{\mu\nu\rho\sigma}B^{\rho\sigma} \ , \quad \widetilde{W}^k_{\mu\nu} = \frac{1}{2}\epsilon_{\mu\nu\rho\sigma}W^{\rho\sigma k} \ , \quad \widetilde{G}^a_{\mu\nu} = \frac{1}{2}\epsilon_{\mu\nu\rho\sigma}G^{\rho\sigma a} \ . \tag{2.15}$$

CPV operators can be defined in terms of the mass eigenstates after EWSB (Higgs boson, W, Z, photon, etc.) as follows.

$$\mathcal{L}_{CPV} = -\frac{1}{4}\tilde{g}_{hgg}G^a_{\mu\nu}\tilde{G}^{\mu\nu}h - \frac{1}{4}\tilde{g}_{h\gamma\gamma}F_{\mu\nu}\tilde{F}^{\mu\nu}h - \frac{1}{4}\tilde{g}_{hzz}Z_{\mu\nu}\tilde{Z}^{\mu\nu}h - \frac{1}{2}\tilde{g}_{haz}Z_{\mu\nu}\tilde{F}^{\mu\nu}h - \frac{1}{2}\tilde{g}_{hww}W^{\mu\nu}\tilde{W}^\dagger_{\mu\nu}h \tag{2.16}$$

D6 operators of the effective couplings in mass and gauge basis are given in Table 2.1.(Giudice et al., 2007), (Contino et al., 2013),

In the past CPV Higgs-gauge boson coupling via HDO were carried out both experimentally at LHC (Aaboud et al., 2018; Aad et al., 2016; Sirunyan et al., 2019b,a) and phenomenologically at LHC (Desai et al., 2011; Godbole et al., 2014; Brod et al., 2013; Bernlochner et al., 2019) at HE-LHC and HL-LHC (Ferreira et al., 2017; Dwivedi et al., 2016; Cepeda et al., 2019) at future e^+e^- (Rao and Rindani, 2006; Biswal and Godbole,

Table 2.1. Vector boson pair and the Higgs boson interactions coupling strength (Alloul et al., 2014b).

Eq. 2.16	Section 2.2
g_{hgg}	$g_H - \frac{4\bar{c}_g g_s^2 v}{m_W^2}$
$\tilde{g}_{hgg}$	$-\frac{4\tilde{c}_g g_s^2 v}{m_W^2}$
$g_{h\gamma\gamma}$	$a_H - \frac{8g\bar{c}_\gamma s_W^2}{m_W}$
$\tilde{g}_{h\gamma\gamma}$	$-\frac{8g\tilde{c}_\gamma s_W^2}{m_W}$
$g_{hzz}^{(1)}$	$\frac{2g}{c_W^2 m_W}\left[\bar{c}_{HB} s_W^2 - 4\bar{c}_\gamma s_W^4 + c_W^2 \bar{c}_{HW}\right]$
$\tilde{g}_{hzz}$	$\frac{2g}{c_W^2 m_W}\left[\tilde{c}_{HB} s_W^2 - 4\tilde{c}_\gamma s_W^4 + c_W^2 \tilde{c}_{HW}\right]$
$g_{hzz}^{(2)}$	$\frac{g}{c_W^2 m_W}\left[(\bar{c}_{HW} + \bar{c}_W) c_W^2 + (\bar{c}_B + \bar{c}_{HB}) s_W^2\right]$
$g_{hzz}^{(3)}$	$\frac{g m_W}{c_W^2}\left[1 - \frac{1}{2}\bar{c}_H - 2\bar{c}_T + 8\bar{c}_\gamma \frac{s_W^4}{c_W^2}\right]$
$g_{haz}^{(1)}$	$\frac{g s_W}{c_W m_W}\left[\bar{c}_{HW} - \bar{c}_{HB} + 8\bar{c}_\gamma s_W^2\right]$
$\tilde{g}_{haz}$	$\frac{g s_W}{c_W m_W}\left[\tilde{c}_{HW} - \tilde{c}_{HB} + 8\tilde{c}_\gamma s_W^2\right]$
$g_{haz}^{(2)}$	$\frac{g s_W}{c_W m_W}\left[\bar{c}_{HW} - \bar{c}_{HB} - \bar{c}_B + \bar{c}_W\right]$
$g_{hww}^{(1)}$	$\frac{2g}{m_W}\bar{c}_{HW}$
$\tilde{g}_{hww}$	$\frac{2g}{m_W}\tilde{c}_{HW}$
$g_{hww}^{(2)}$	$\frac{g}{m_W}\left[\bar{c}_W + \bar{c}_{HW}\right]$

2009; Beneke et al., 2014; Amar et al., 2015; Kumar et al., 2015) and ep (Biswal et al., 2012) colliders. In this thesis, the impacts of CPV D-6 operators of HWW, $H\gamma\gamma$ and HZZ vertices were studied which described by SM EFT approach in $e^+e^- \to H\nu\bar{\nu}$ process at three energy stages of CLIC.

3. CLIC OVERVIEW

CLIC is a 50 km, multi-TeV high-luminosity linear e^+e^- collider which is in the research and development stage with international collaborations at CERN. CLIC will be built in three center-of-mass energy stages to complement the LHC results and cover the widest possible physical opportunities. The baseline staging scenario assumes that the program will span 25-30 years for three energy stages which are $\sqrt{s}$ = 380 GeV, 1.5 TeV and 3 TeV and the luminosities correspond for these three energy stages 1.0 ab^{-1}, 2.5 ab^{-1}, 5.0 ab^{-1} respectively. The illustration of these three stages are shown (Figure 3.1). The collisions at first energy stage will provide rich programme for precision measurement of top quark which so far has been only produced in hadron collisions, and Higgs boson that will reach and unique Higgs physics program.

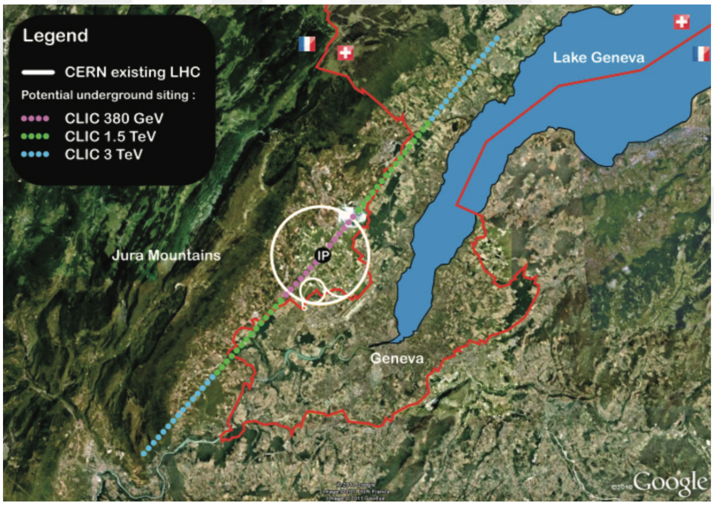

Figure 3.1. CLIC is a future option for post-LHC collider.

To go further up, the machine will be reached the higher energies (1.5 TeV and 3 TeV) and it provides unique sensitivities for new physics scenarios and gives access the Higgs potential through the measurement of the Higgs self-coupling.

Schematic configuration of CLIC two-beam accelerator is shown (Figure 3.2). Electrons and positrons emittance is reduced in damping rings. They accelerate the beam to 9 GeV and delivers them to the main linacs. The main linacs accelerate both beams with the accelerating gradient of 72 MV/m to the collision center-of-mass energy of 190 GeV.

In order to reach multi-TeV center-of-mass energies, the X-band accelerating structures are used to get 100 MV/m gradient capability.

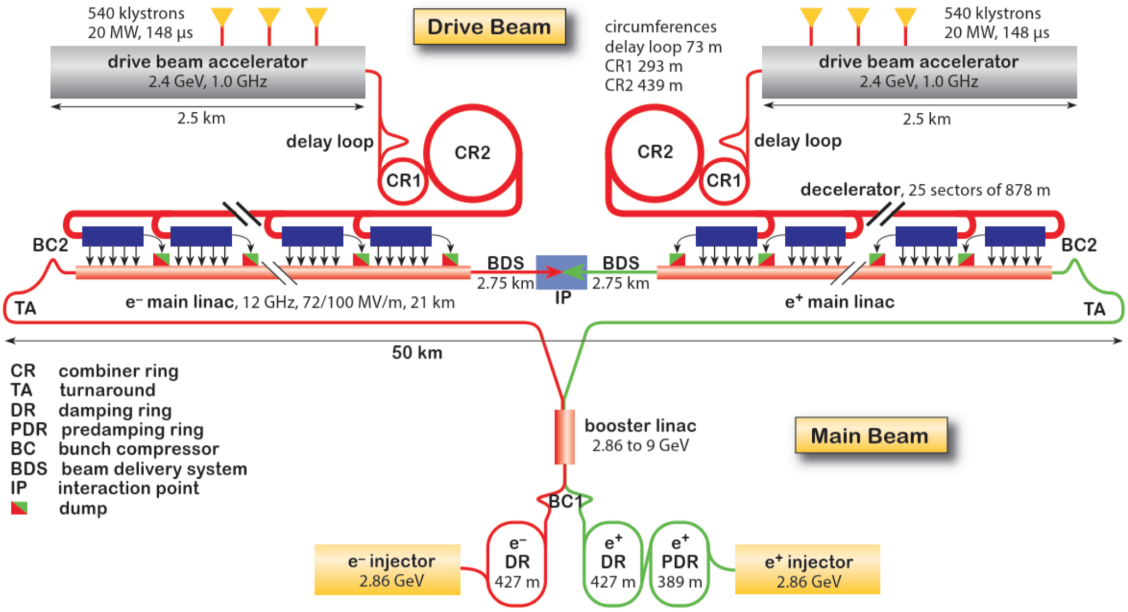

Figure 3.2. The proposed layout for CLIC, showing the various components of the injection system and the drive-beam system (not to scale).

For having a high gradient, the accelerating structures need very high power radio-frequency (RF) pulses.These required RF pulses are obtained from novel drive-beams which are parallel to the main beam. This drive-beams power is extracted and converted to RF power by a special device which is called Power Extraction and Transfer Structures (PETS) is shown (Figure 3.3). This two-beam acceleration method provides high efficiencies with low costs.

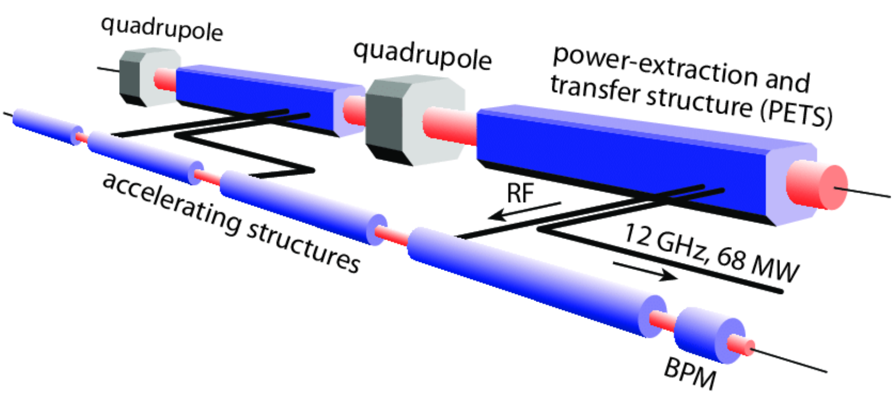

Figure 3.3. The CLIC two-beam scheme, with the main beam accelerated by energy provided from the lower-energy, high-current drive beam.

To understand and explore new physics BSM in TeV energy range is needed to get stringent requirements on the detector performance. Here the performance is meant by vertex reconstruction, particle identification, precise momentum resolution, jet reconstruction and hermetic coverage and so on. Two detector models $CLIC_I LD$ and $CLIC_S iD$ were purposed which are based on the concept for ILC detector and adapted to center-of-mass energies from 380 GeV to 3 TeV. The most distinctive features for CLIC, it has higher center-of-mass energy than ILC and 0.5 ns between bunch crossing at CLIC. Higher energies lead to more background from incoherent pairs and more hadronic two-photon events mostly in forward regions. Particle production in the t-channel with particles in the forward region become more important and jets will be more narrow in the detector due to a stronger boost. The ILD and SiD designs are modified to meet the CLIC performance requirements. The design principles of CLIC detector, based on ILC detector concept

- Effective tracking detectors with well reconstruction of momentum in a solenoid with high field;
- reconstruction of secondary vertex with precise pixel detector near the beam pipe;
- low cost of tracking devices;
- highly segmented hadronic and electromagnetic calorimeters in the solenoid;
- detector hermecity which is very important for determining of missing energy, major sign of new physical processes;
- instrumented return yoke for muon identification;

The CLIC enable to probe wide range of physics opportunities with its clean experimental environment and well-known initial state. Observing the rare processes can be possible at all the energy stages of CLIC by the absence of QCD background and having high luminosity. Threshold scans ensure measurement of masses of known particles precisely. So far particle physics experiments including LHC can not answer the many question about particles and their interactions and it seems unlikely that the hint of new physics can be observed on the current energy scale and also even for HL-LHC. In this context, CLIC can open the door for BSM searches and provide observation of unexplored territories of physics. (Linssen et al., 2012; Charles et al., 2018; Robson and Roloff, 2018; Roloff et al., 2018; Aicheler et al., 2012).

Figure 3.4. CLIC is a future option for post-LHC collider.

4. AIM AND SCOPE OF THE STUDY

The main purpose of this thesis is to represent the effects of CPV D6 operators through $e^+e^- \rightarrow \nu\bar{\nu}H$ process in Effective Field Theory (EFT) framework. These effects are examined at the three energy stages of Compact Linear Collider (CLIC) which is one of the mature option with its clean environment among the future colliders, plan to build at Conseil Européen pour la Recherche Nucléaire (CERN) in Geneva, Switzerland.

5. MATERIALS AND METHODS

5.1 Event Generation

The goal of this thesis, is to emphasize the sensitivity of CLIC at three energy stages for $\tilde{c}_{HW}$, $\tilde{c}_{HB}$ and $\tilde{c}_{\gamma}$ couplings. To do this the impact of CPV D6 operators via $e^+e^- \to \nu\bar{\nu}H$ process were investigated with using the method of Monte Carlo (MC) simulation `MadGraph5_aMC_v2.6.3.2@NLO` (Alwall et al., 2014). The expression of CPV operators In Eq. 2.14 were defined into the `MadGraph5_aMC_v2.6.3.2@NLO` based on FeynRules (Alloul et al., 2014a) and the UFO (Degrande et al., 2012). In Figure 5.1 the cross section distribution were shown for $e^+e^- \to \nu\bar{\nu}H$ process with respect to $\tilde{c}_{HW}$, $\tilde{c}_{HB}$ and $\tilde{c}_{\gamma}$ couplings for all energy stages of CLIC. These cross sections at generator level do not involve the ISR and beamsstrahlung effects. The quartic contributions that we mentioned in Sec. 1.5 were considered, when a coefficient is changed in cross section calculation.

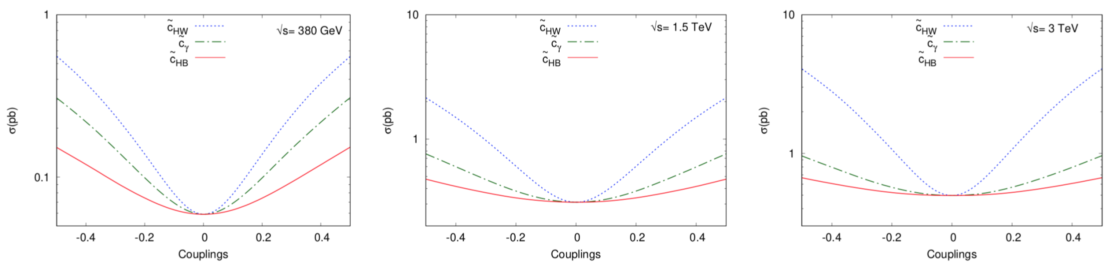

Figure 5.1. The total cross section as a function of CP-violating $\tilde{c}_{HW}$, $\tilde{c}_{HB}$ and $\tilde{c}_{\gamma}$ couplings for $e^+e^- \to \nu\bar{\nu}H$ process at the CLIC with $\sqrt{s}$=380 GeV, $\sqrt{s}$=1.5 TeV and $\sqrt{s}$=3 TeV.

Table 5.1. The cross section values for backgrounds in pb.

$\sqrt{s}$	B_H	B_{ZZ}	B_{WW}	$B_{t\bar{t}}$	$B_{Z\nu\nu}$
380 GeV	0.059	0.597	10.229	0.618	0.419
1.5 TeV	0.310	0.079	1.437	0.079	1.339
3 TeV	0.497	0.026	0.47	0.020	2.16

In the analysis, several coupling constant values were taken into account for $\tilde{c}_{HW}$, $\tilde{c}_{HB}$ and

$\tilde{c}_\gamma$ couplings through $e^+e^- \to \nu\bar{\nu}H$ process and in final states we focused on $H \to b\bar{b}$ decay channel. With taking these values were very small, the effect of CPV D6 operators on decay width were very close to SM. So the contribution of these operators could be neglected for branching ratio (BR) of $H \to b\bar{b}$ final states.

Since the final state of the signal was $H \to b\bar{b}$, all relevant backgrounds were chosen with respect to this decay channel. First background was SM (B_H) which had same final states with signal and only SM contributions were considered. Second background was $e^+e^- \to ZZ$ process (B_{ZZ}) that one Z decayed to $b\bar{b}$ and another decayed to $\nu\bar{\nu}$. The following one was $e^+e^- \to W^+W^-$ background process (B_{WW}) that was dominant in all mass region of the Higgs boson. One W boson decayed hadronically ($q\bar{q}'$) and another one decayed leptonically ($l\nu$). The fourth background was top pair production ($e^+e^- \to t\bar{t}$). It was the one of the major background that was hard to discriminate from signal. Final states for this background was $t \to W^+b$ and $\bar{t} \to W^-\bar{b}$ with the number of two b-jets. Last background was $e^+e^- \to \nu\bar{\nu}Z$ process ($B_{Z\nu\nu}$) that Z decayed hadronically. Moreover, an irreducible background contribution from $e\gamma$ and $\gamma\gamma$ collision could be expected to see but in this analysis we neglected them because in these collision events that contains photons from Beamstrahlung, did not produce via Madgraph. The cross sections of these relevant backgrounds are shown (Table 5.1).

BTag value	7	6	5	4	3	2	1	0
BTag binary	111	110	101	100	011	010	001	000
(bit 0) & BTag	T	F	T	F	T	F	T	F
(bit 1) & BTag	T	T	F	F	T	T	F	F
(bit 2) & BTag	T	T	T	T	F	F	F	F

Figure 5.2. The combinations of b-tagging algorithm for tuned CLIC detector card (Leogrande et al., 2019).

500k events produced for each signals and backgrounds with using MC event generator program `MadGraph5_aMC_v2.6.3.2@NLO` that can simulate the physical events of particle same as nature. Then all produced events passed through PYTHIA 8.2 which provides a definitions for hadronization, parton shower and decay of unstable particles (Sjöstrand

Table 5.2. Event selection criteria and applied kinematic cuts used for the analysis at three energy stages of CLIC

Cuts	$\sqrt{s}$ =380 GeV
Cut-0	Jet clustering: VLC with $\beta = \gamma = 1.0$ R=1.0 Exclusive clustering with $N_j = 2$ Jets energy scale is assumed to be 1.0 lepton vetos, MET> 0
Cut-1	requiring two b-tagged jets
Cut-2	$\eta^{b1,b2} \leqslant 2.0$, $p_T^{b1} > 50$ GeV, $p_T^{b2} > 30$ GeV $\not{E}_T > 30$ GeV
Cut-3	100 GeV $< H_T <$ 200 GeV
Cut-4	96 GeV $< M_{(b\bar{b})} < 136$ GeV
Cut-5	$p_T^{b\bar{b}} > 75$ GeV

et al., 2015). For realistic detector response we used a tuned CLIC detector card that designed for three energy stages of CLIC, implemented in Delphes 3.4.1 version (de Favereau et al., 2014). In this card jets were clustered in exclusive mode (Boronat et al., 2015b) by Valencia Linear Collider (VLC) algorithm (Boronat et al., 2015a) that concerted with the environment of linear colliders. The VLC was applied with using FastJet (Cacciari et al., 2012) $\beta = \gamma = 1.0$ and fixed number of jets ($N = 2, 3, 4, 5, 6$) and five different combinations of jet cone size ($R = 0.5, 0.7, 1.0, 1.2, 1.5$). Three working points (WP) of b-tagging efficiencies and corresponding mis-tagging rates are implemented in CLICdet card (Leogrande et al., 2019). There are three defined efficiencies for b-tagging which are loose WP with 90%, medium WP with 70% and tight WP with 50%. In Figure 5.2 the combinations of different bits to choose the WP is shown. To work with 50% b-tagging efficiency (tight WP) bit0 i.e. 1, 3, 5, 7 combinations were selected in C++ macro code. For working with 70% b-tagging efficiency (medium WP) bit1 corresponds to 2, 3, 6 and 7, for working with 90% b-tagging efficiency (loose WP) corresponds to bit2 and its combinations BTag $\geq$ 4 must be selected.Finally data structures for all events were in "trees" format that included information of produced signal and background events. These datas were analyzed with using the ExROOT package (ExRootAnalysis, 1999) that was designed for facilitating ROOT 6.16 (Brun and Rademakers, 1997) tree production.

5.2 $\sqrt{s}$ = 380 GeV

In this part of the analysis, considering Fig. 5.1 $\tilde{c}_{HW}$= 0.01, 0.03, 0.05, 0.08

Table 5.3. Number of signal for $\tilde{c}_{HW}$=0.1 and relevant backgrounds events after applied kinematic cuts used for the analysis at $\sqrt{s}$ = 380 GeV with $L_{int} = 1$ ab^{-1} for the three working point of b-tagging efficiency.

Cuts	b-tagging eff.	$S + B_H$	B_H	B_{ZZ}	B_{tt}	$B_{Z\nu\nu}$	B_{WW}
no cut	-	76700	57393	363009	522879	308233	
Cut-0	-	69134	51743	288932	314891	298485	3059160
Cut-1	50%	10206	7664	10565	14861	13763	143
	70%	20007	15036	20669	29643	27411	307
	90%	33523	25086	39704	62056	49403	28764
Cut-2	50%	5376	3912	3004	6286	3963	82
	70%	10570	7637	5950	12271	7883	82
	90%	17679	12669	10534	24136	14007	1657
Cut-3	50%	5130	3716	2603	2027	3360	61
	70%	10074	7253	5115	3797	6613	82
	90%	16858	12025	8891	7351	11736	1350
Cut-4	50%	4322	3162	131	776	144	-
	70%	8470	6171	225	1464	268	-
	90%	14169	10207	432	2963	522	123
Cut-5	50%	2971	1959	122	393	116	-
	70%	5815	3842	195	768	207	-
	90%	9691	6352	381	1427	417	20

and 0.1, $\tilde{c}_{HB}$= 0.05, 0.08, 0.1, 0.3 and 0.5, $\tilde{c}_{\gamma}$= 0.05, 0.08, 0.1, 0.2 and 0.3 signal events were generated. Kinematical cuts in Table 5.2 were used to separate signal events from the relevant background events and these cuts applied step by step for detail cut base analysis. First selection is jet clustering (i.e, N_{jets}=2 and R=1.0) and no charged leptons are selected (Cut-0). From this selection we had two jets which were coming from decay of the Higgs boson and these jets were tagged as b-tagged. The b-tagged jets were labelled b1 and b2 with respect to higher transverse momentum (p_T) (cut-1).

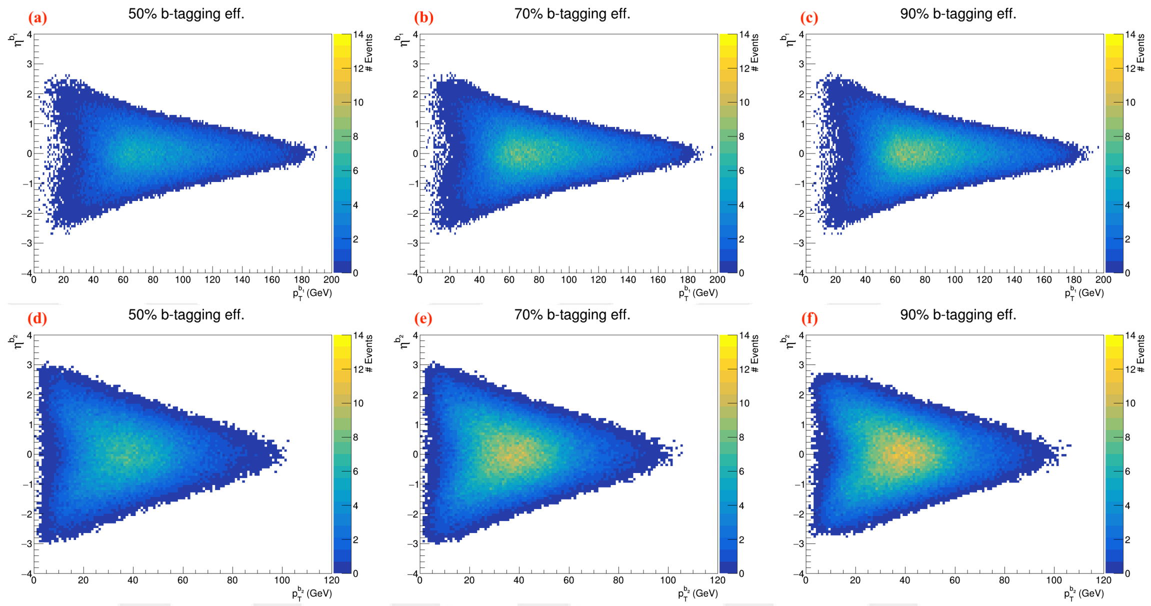

Figure 5.3. The pseudo-rapidity versus transverse momentum distribution of leading ($b1$) and sub-leading ($b2$) b-tagged jets for SM $e^+e^- \to \nu\bar{\nu}H$ process with defined three efficiency working points (50 %, 70 % and 90 %) in CLIC Delphes card at $\sqrt{s}$=380 GeV. a) 50 % for η_{b_1} vs $p_T^{b_1}$ b) 70 % for η_{b_1} vs $p_T^{b_1}$ c) 90 % for η_{b_1} vs $p_T^{b_1}$ d) 50 % for η_{b_2} vs $p_T^{b_2}$ e) 70 % for η_{b_2} vs $p_T^{b_2}$ f) 90 % for η_{b_2} vs $p_T^{b_2}$.

Figure 5.3 was shown the transverse momentum (p_T) vs pseudo rapidity (η) distributions of SM background for first energy stage of the CLIC with three b-tagging working points (50% 70% 90%) which implemented in Delphes Card as mentioned before. For the analysis, loosely working point (90%) were considered because 90% b-tagging efficiency provided more events than medium (70%) and tight (50%) working points. Next cut contained various constraints which were $b1$ with $p_T^{b1} > 50$ GeV and $b2$ with $p_T^{b2} > 30$ GeV and pseudo-rapidity of the b-tagged jets to be $|\eta^{b1,b2}| \leq 2.0$ and missing energy transverse (MET) (undetected particle energies in the detector) $\not{E}_T > 30$ GeV (cut-2). The useful quantity for this analysis is the scalar scalar transverse energy sum (H_T). The definition of H_T is $H_T = \sum_i |\vec{p_T}(i)|$.

Here i is the selected input collections (de Favereau et al., 2014). This cut requiring to be 100 GeV $< H_T <$ 200 GeV (Cut-3). Following cut was the invariant mass region of reconstructed Higgs-boson from two b-jets were taken to be 96 GeV $< M_{(b\bar{b})} <$ 136 GeV (Cut-4). The final cut was the transverse momentum of reconstructed Higgs-boson from two b-jets $p_T^{bb} >$ 75 GeV that was used to obtain limits on $\tilde{c}_{HW}$, $\tilde{c}_{HB}$ and $\tilde{c}_{\gamma}$ couplings (Cut-5). The effects of these cuts on relevant background and signal events were discussed in detail with figures and integral values which referred to number of events bin by bin.

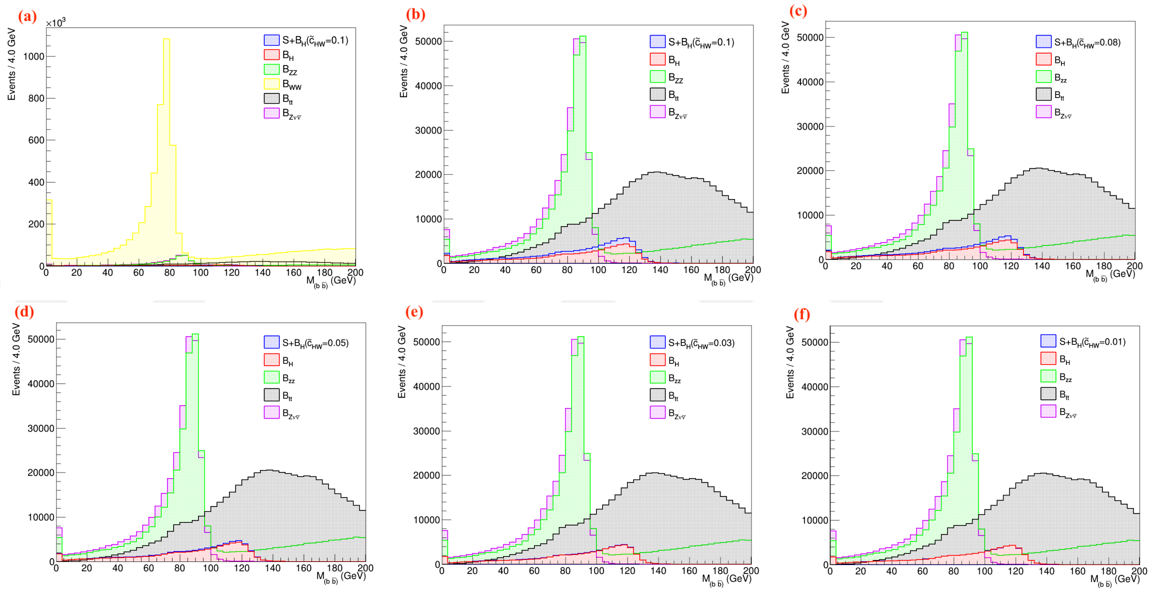

Figure 5.4. Normalized distributions of invariant mass of Higgs, reconstructed from two b-tagged jets for all signal events and all backgrounds with no cut. a) $\tilde{c}_{HW}$ = 1.0 with B_{WW} background. b) $\tilde{c}_{HW}$ = 1.0 without B_{WW} background. c) $\tilde{c}_{HW}$ = 0.08 without B_{WW} background. d) $\tilde{c}_{HW}$ = 0.05 without B_{WW} background. e) $\tilde{c}_{HW}$ = 0.03 without B_{WW} background. f) $\tilde{c}_{HW}$ = 0.01 without B_{WW} background.

At the beginning, all background events were much more dominant than signal events (Figure 5.4). Especially in Figure 5.4(a) B_{WW} were suppressed other background and signals, so it was dropped from other figures only in this part for simplicity. When looked at the mass range of the Higgs which was from 96 GeV to 136 GeV, it can be said that, especially $t\bar{t}$ background was very effective in that region. In addition, the behavior of SM background was almost same with the behavior of all signals except for $\tilde{c}_{HW}$= 0.1. So it was selected as reference signal for the analysis. In same way we selected other backgrounds B_{ZZ} and $B_{Z\nu\nu}$ that peaked at their mass region of Z boson as expected.First of all, to separate the signal from backgrounds, cut-0 (N_{jets}=2 and R=1.0) were used.

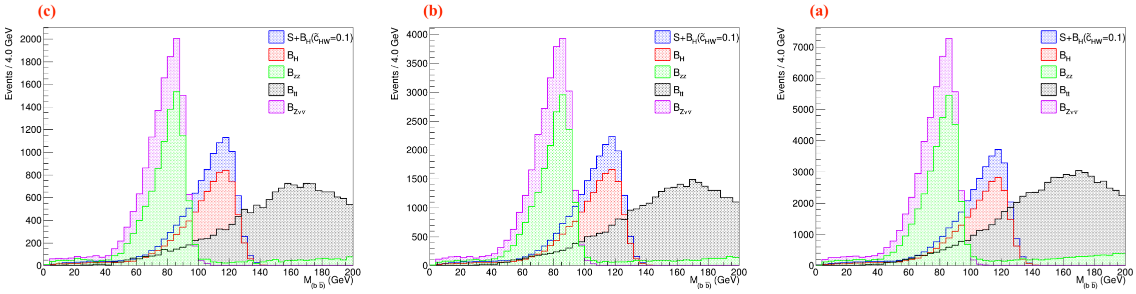

Figure 5.5. Normalized distributions of invariant mass of the Higgs for three b-tagging working points for $\tilde{c}_{HW}$= 0.1. a) for 50 % b-tagging WP b) for 70 % b-tagging WP c) for 90 % b-tagging WP

From Table 5.3 almost same amount of number of events were removed for $S + B_H$ and B_H after using this cut. Maximum effect of cut-0 was on $t\bar{t}$ background, removed nearly 39% of its events. In Figure 5.5 the invariant mass distribution of Higgs were illustrated after cut-1 for three different b- tagging working points 90%, 70%, 50% respectively.

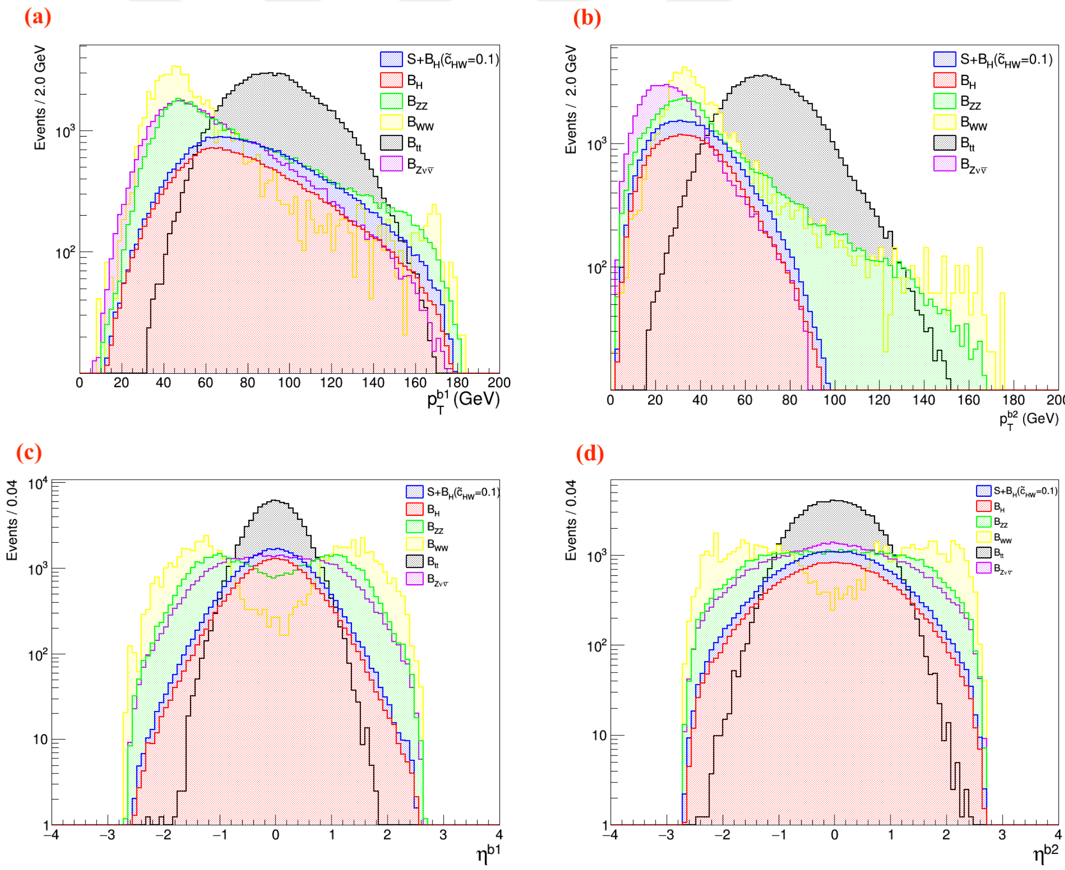

Figure 5.6. Normalized distributions of transverse momentum, pseudo-rapidity of tagged b-jets at $\sqrt{s}$ =380 GeV for signal with $\tilde{c}_{HW} = 0.1$ and relevant background processes after cut1. a) $p_T^{b_1}$ b) $p_T^{b_2}$ c) η_{b_1} d) η_{b_2}

For 90% b-tagging efficiency signal and SM background lost almost the half of their events and reduced the number of events for other backgrounds drastically.Medium WP (70%) and tight WP (50%) b-tagging efficiencies were suppressed all signal and background events more than loosely WP (90%) so next figures were illustrated with 90%. Next, Figure 5.6 (c), (d) and Figure 5.8 and Figure 5.9 η distributions for leading $(b1)$ and sub-leading $(b2)$ b-tagged jets were shown. From Figure 5.6 (a) and Figure 5.10 p_T^{b1} required to be greater

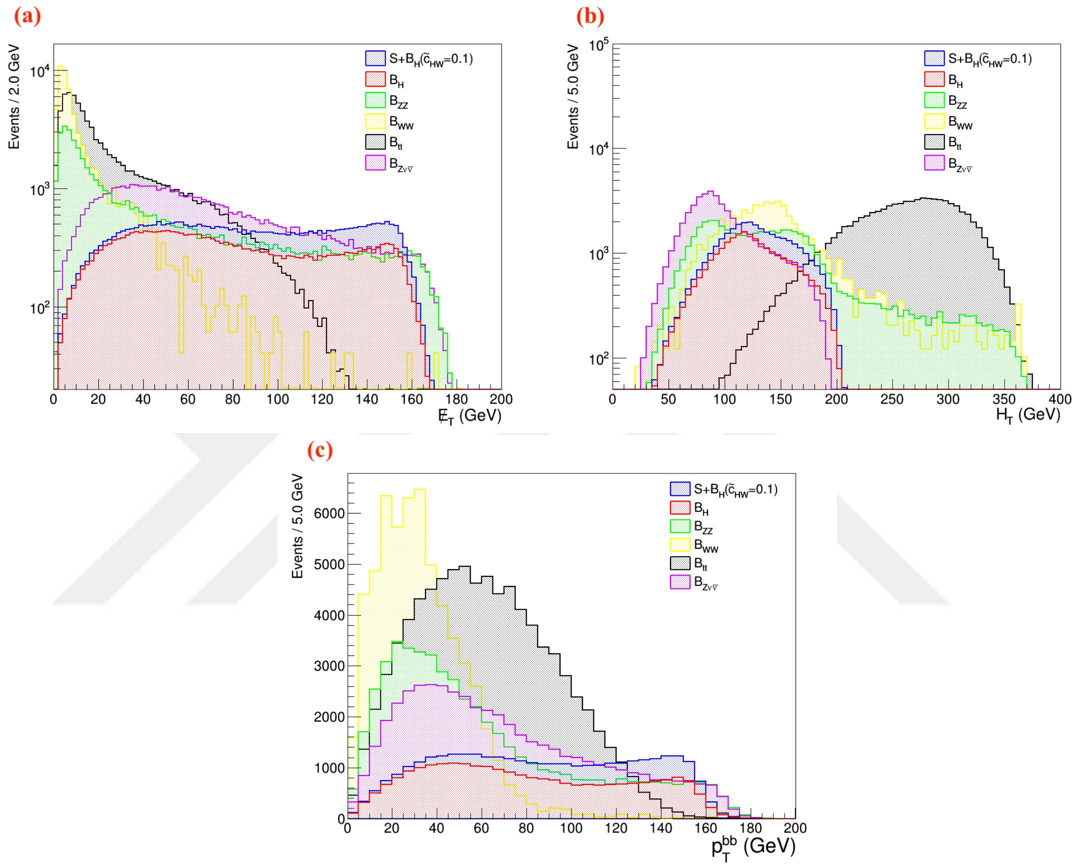

Figure 5.7. Normalized distributions of MET and Scalar Transverse Energy of tagged b-jets, at $\sqrt{s}$ =380 GeV for signal with $\tilde{c}_{HW} = 0.1$ and relevant background processes after cut1. a) $\not{E}_T$ b) H_T c) p_T^{bb}.

than 50 GeV. This cut provided to suppress B_{ZZ}, $B_{Z\nu\nu}$ and B_{WW} background events. To show the effect of this cut in more detail, the number of event values in Table 5.5 were taken into account. From these values, the effectiveness of $p_T^{b1} > 50$ GeV cut can be represented in percentages for $S + B_H$, B_H, B_{ZZ}, B_{tt}, $B_{Z\nu\nu}$ and B_{WW} which were 11%, 13%, 28%, 1.7%, 31% and 59% respectively.

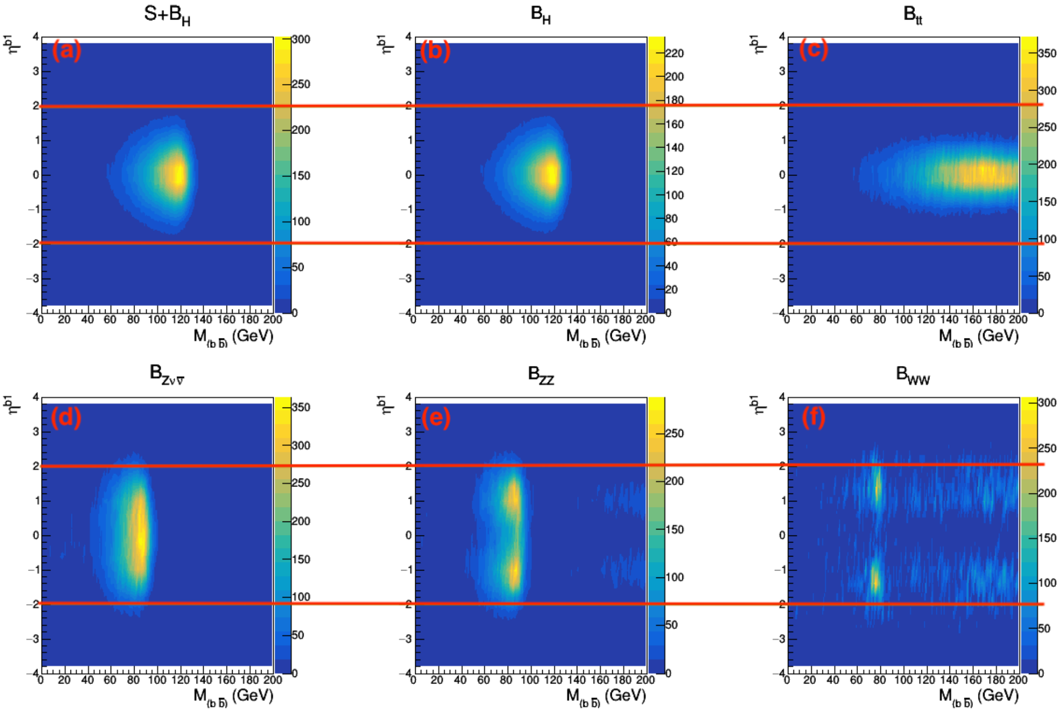

Figure 5.8. η distribution of leading $(b1)$ jet versus invariant mass of reconstructed Higgs from b-tagged jets for (a) $S + B_H$ ($\tilde{c}_{HW}$=0.1) (b)B_H (c)B_{tt} (d)$B_{Z\nu\nu}$ (e)B_{ZZ} (f)B_{WW} .

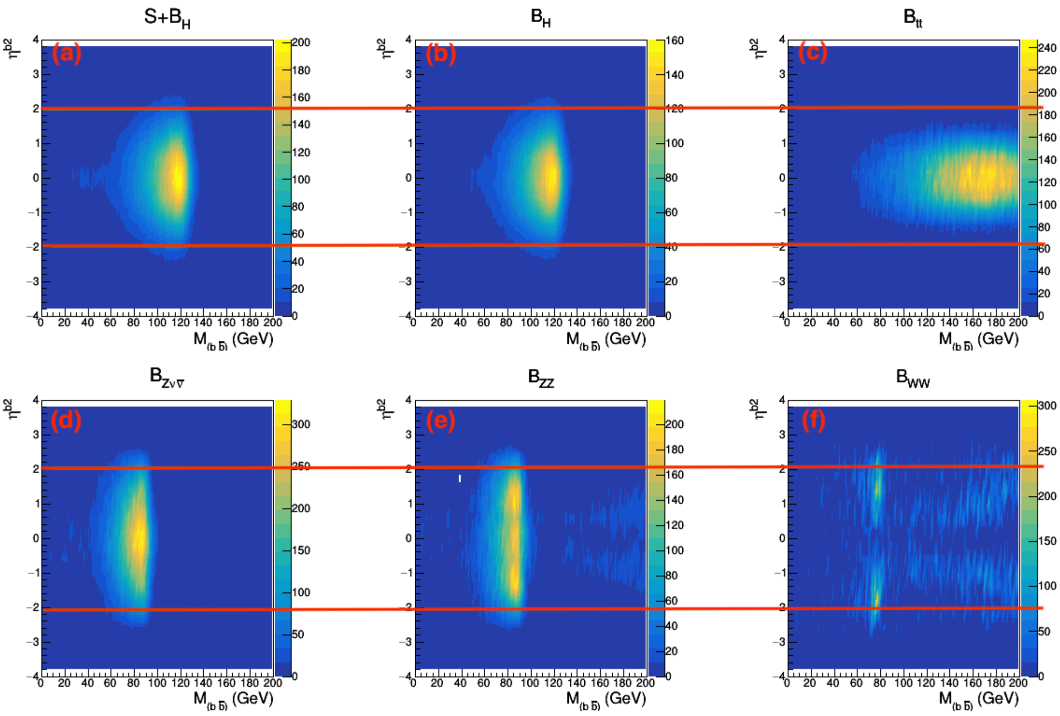

Figure 5.9. η distribution of sub-leading $(b2)$ jet versus invariant mass of reconstructed Higgs from b-tagged jets for (a) $S + B_H$ ($\tilde{c}_{HW}$=0.1) (b)B_H (c)B_{tt} (d)$B_{Z\nu\nu}$ (e)B_{ZZ} (f)B_{WW}.

Table 5.4. Number of signal for $\tilde{c}_{HW}$=0.1 and relevant backgrounds events after $\eta^{b1,b2} \leqslant 2.0$ cut used for the analysis at $\sqrt{s}$ = 380 GeV with $L_{int} = 1$ ab^{-1} for loosely (90 %) of b-tagging efficiency.

Cuts	$S + B_H$	B_H	B_{ZZ}	B_{tt}	$B_{Z\nu\nu}$	B_{WW}
no cut	76700	57393	363009	522879	308233	6393290
Cut-0	69134	51743	288932	314891	298485	3059160
Cut-1	33523	24965	39704	62056	49403	28563
$\eta^{b1,b2} \leqslant 2.0$	32381	24168	35138	62011	44868	21563

Table 5.5. Number of signal for $\tilde{c}_{HW}$=0.1 and relevant backgrounds events after $p_T^{b1} > 50$ GeV cut used for the analysis at $\sqrt{s}$ = 380 GeV with $L_{int} = 1$ ab^{-1} for loosely (90 %) of b-tagging efficiency.

Cuts	$S + B_H$	B_H	B_{ZZ}	B_{tt}	$B_{Z\nu\nu}$	B_{WW}
$\eta^{b1,b2} \leqslant 2.0$	32381	24168	35138	62011	44868	21563
$p_T^{b1} > 50$ GeV	28563	20817	24967	60901	30756	8858

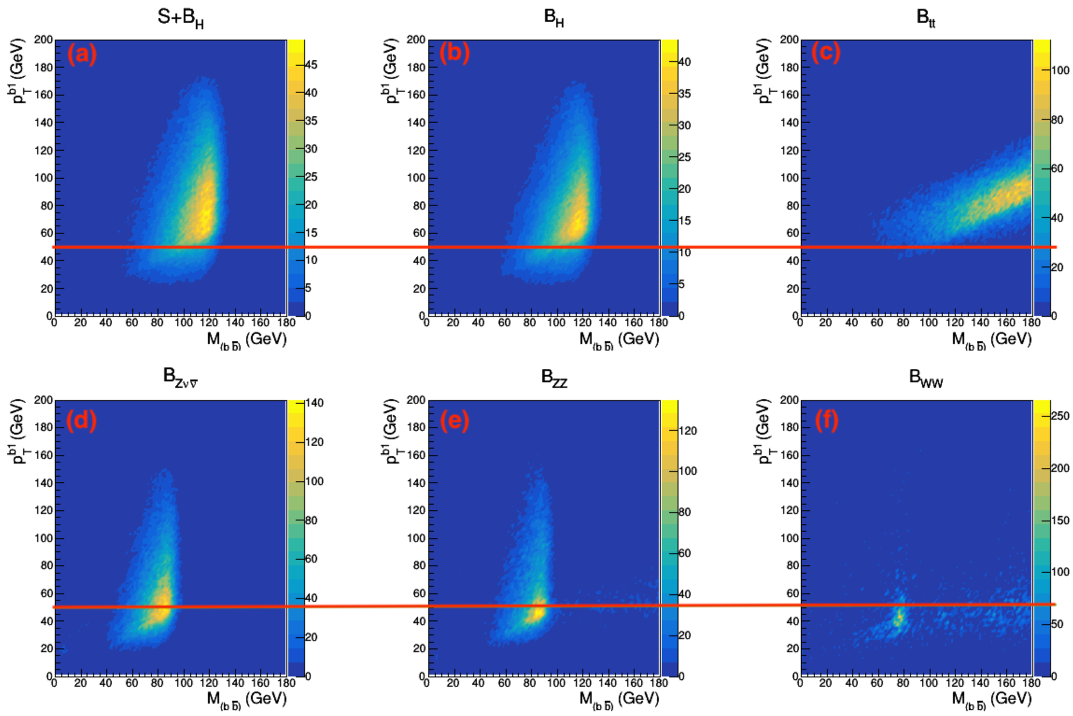

Figure 5.10. p_T of leading $(b1)$ jet versus invariant mass distribution of reconstructed Higgs from b-tagged jets for (a) $S + B_H$ ($\tilde{c}_{HW}$=0.1) (b)B_H (c)B_{tt} (d)$B_{Z\nu\nu}$ (e)B_{ZZ} (f)B_{WW}.

Table 5.6. Number of signal for $\tilde{c}_{HW}$=0.1 and relevant backgrounds events after $p_T^{b2} > 30$ GeV cut used for the analysis at $\sqrt{s}$ = 380 GeV with $L_{int} = 1$ ab^{-1} for loosely (90 %) of b-tagging efficiency.

Cuts	$S + B_H$	B_H	B_{ZZ}	B_{tt}	$B_{Z\nu\nu}$	B_{WW}
$p_T^{b1} > 50$ GeV	28563	20817	24967	60901	30756	8858
$p_T^{b2} > 30$ GeV	19273	14105	15510	60350	14509	6874

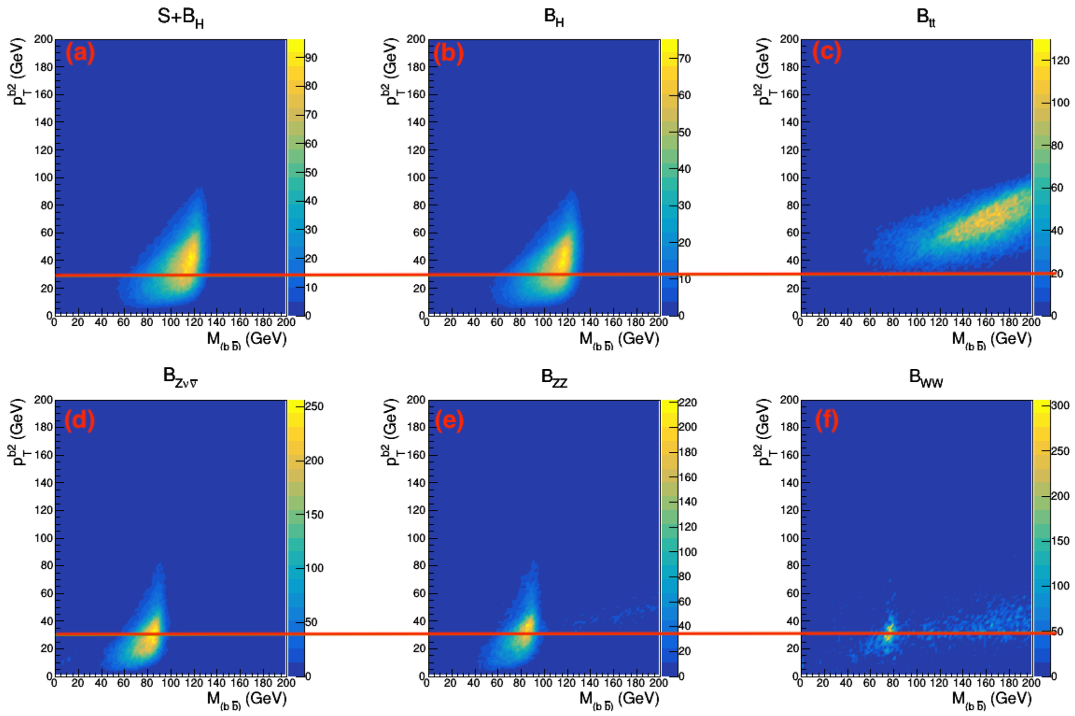

Figure 5.11. p_T of sub-leading $(b2)$ jet versus invariant mass distribution of reconstructed Higgs from b-tagged jets for (a) $S + B_H$ ($\tilde{c}_{HW}$=0.1) (b)B_H (c)B_{tt} (d)$B_{Z\nu\nu}$ (e)B_{ZZ} (f)B_{WW}.

According to Figure 5.6 (b) and Figure 5.11 p_T^{b2} cut required to be greater than 30 GeV. At first glance, it can be said that this operation destroyed more events from signal than SM, but this operation was effective on backgrounds events which contain Z boson especially $B_{Z\nu\nu}$. Again given the effectiveness of this cut in the percentages $S + B_H$, B_H, B_{ZZ}, B_{tt}, $B_{Z\nu\nu}$ 11%, 13%, 28%, 1.7%, 31% and 59%.

Table 5.7. Number of signal for $\tilde{c}_{HW}$=0.1 and relevant backgrounds events after $\not{E}_T > 30$ GeV cut used for the analysis at $\sqrt{s}$ = 380 GeV with $L_{int} = 1$ ab^{-1} for loosely (90 %) of b-tagging efficiency.

Cuts	$S + B_H$	B_H	B_{ZZ}	B_{tt}	$B_{Z\nu\nu}$	B_{WW}
$p_T^{b2} > 30$ GeV	19273	14105	15510	60350	14509	6874
$\not{E}_T > 30$ GeV	17679	12644	10534	24136	14007	1657

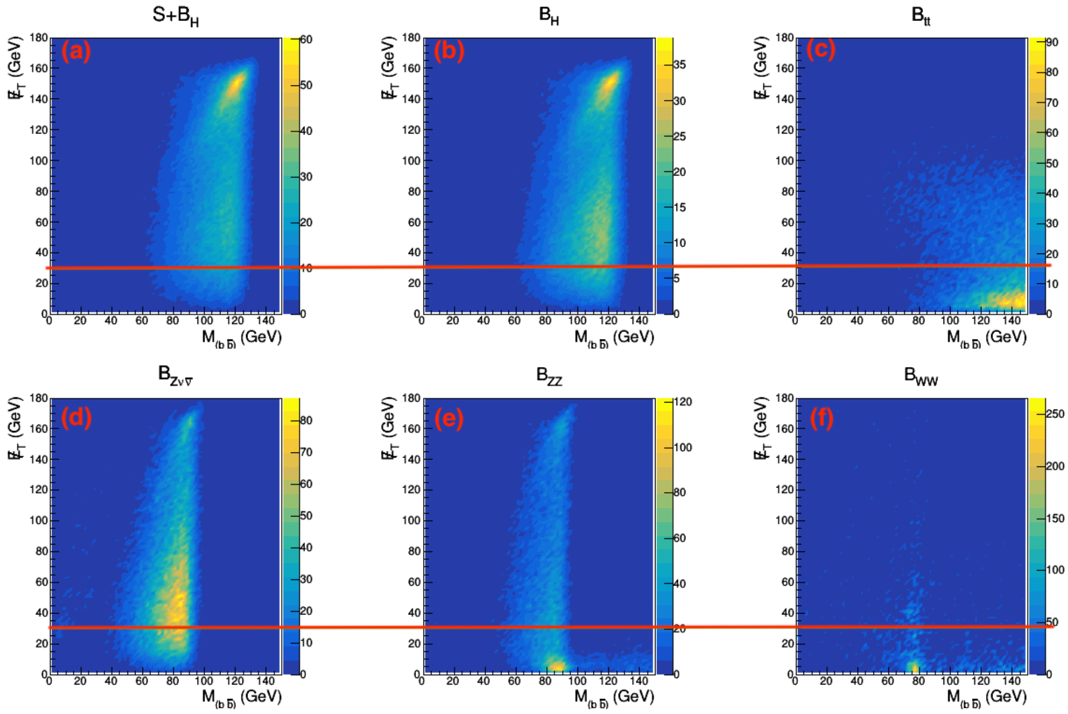

Figure 5.12. MET versus invariant mass distribution of reconstructed Higgs from b-tagged jets for (a) $S + B_H$ ($\tilde{c}_{HW}$=0.1) (b)B_H (c)B_{tt} (d)$B_{Z\nu\nu}$ (e)B_{ZZ} (f)B_{WW}.

The following operation was $\not{E}_T > 30$ GeV, the goal of this cut was intended to remove the events at the region with low MET (Figures 5.7 (a) and 5.12). By applying this operation, eliminated 32%, 60%, 75% percentages of events from B_{ZZ}, B_{tt}, B_{WW} backgrounds respectively which also calculated by the number of events (Table 5.7). Considering Figure 5.7(b) and Figure 5.13 optimum values were found for cut-4 which were 100 GeV $< H_T <$ 200 GeV and it reduced drastically B_{tt} background. This cut was so important for the first part of the analysis because B_{tt} was the most dominant background on mass region of the signal. As seen from Table 5.8 it removed 5% percentages of signal events while it removed 70% of B_{tt} background. The final operation was about obtaining limits on three couplings which were $\tilde{c}_{HW}$, $\tilde{c}_{HB}$ and $\tilde{c}_{\gamma}$. p_T values of reconstructed Higgs-boson were used that required to be $p_T^{bb} > 75GeV$. As it can be seen in Figure 5.14, Figure 5.7(c) and Table 5.9, this cut was effected on B_{ZZ}, $B_{t\bar{t}}$, $B_{Z\nu\nu}$ and B_{WW}. In detail it removed almost all number of events from B_{WW} and removed almost same number of events from the signal and SM background. In summary, at the beginning, the most dominant background was B_{WW} in all mass regions. With using cut-1 the number of events of this background dropped below the number of events of the signal.

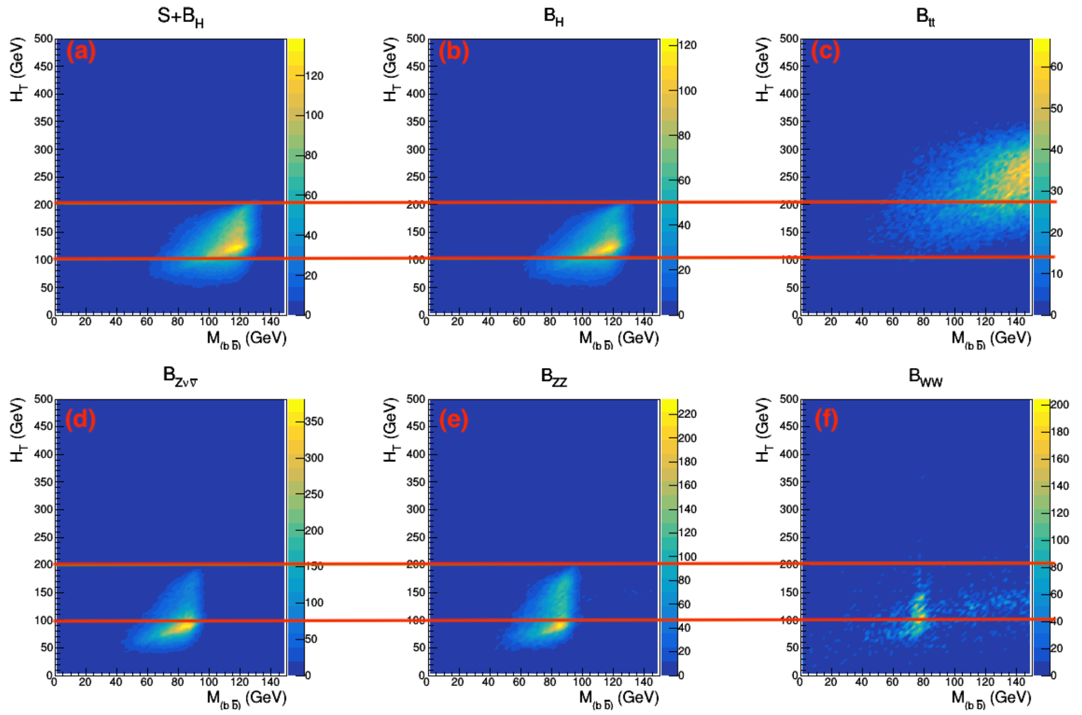

Figure 5.13. Scalar HT versus invariant mass distribution of reconstructed Higgs from b-tagged jets for (a) $S + B_H$ ($\tilde{c}_{HW}$=0.1) (b)B_H (c)B_{tt} (d)$B_{Z\nu\nu}$ (e)B_{ZZ} (f)B_{WW}.

Then we had other dominant backgrounds which are $B_{t\bar{t}}$, B_{ZZ} and $B_{Z\nu\nu}$. Among these, it was important to reduce $B_{t\bar{t}}$ background because it was in the same mass region of the Higgs that we wanted to observe its coupling with other gauge bosons. Especially cut-3 and cut-4 were good choices to suppress it. Finally, cut-5 was used for obtaining better limit that we calculated statistically.

Same cut base work was done for other $\tilde{c}_{HB}$ and $\tilde{c}_{\gamma}$ couplings with their signals that we mentioned at the beginning of this section. As a result, like $\tilde{c}_{HW}$, at 380 GeV center of mass energy, the background events have been able to successfully separate from the signal events for $\tilde{c}_{HB}$ and $\tilde{c}_{\gamma}$. This cut base study was able to separate the signal events from background

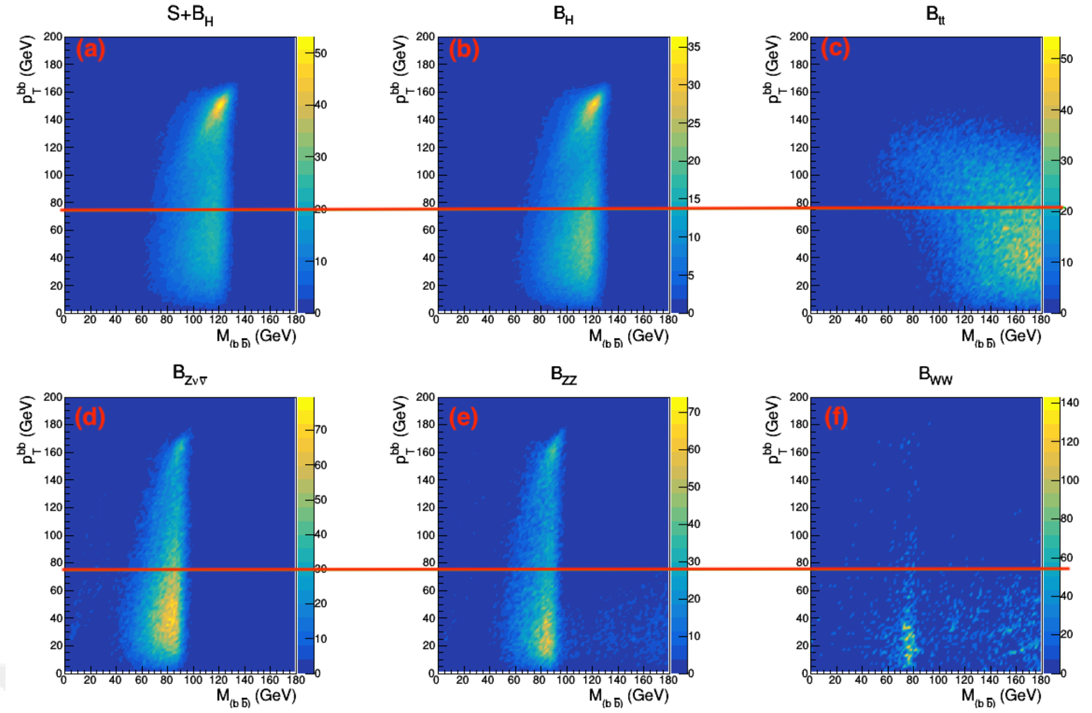

Figure 5.14. Transverse momentum of the Higgs versus invariant mass distribution of reconstructed Higgs from b-tagged jets for (a) $S + B_H$ ($\tilde{c}_{HW}$=0.1) (b)B_H (c)B_{tt} (d)$B_{Z\nu\nu}$ (e)B_{ZZ} (f)B_{WW}.

events with 55% efficiency for the $c_\gamma = 0.2$ signal while working with 60% efficiency for the $\tilde{c}_\gamma = 0.3$ signal. Normalized distribution of three selected signal for each couplings and total background events after cut-4 was shown (Figure 5.14). It can easily say that all dominant backgrounds were suppressed for each coupling at the first energy stage of CLIC.

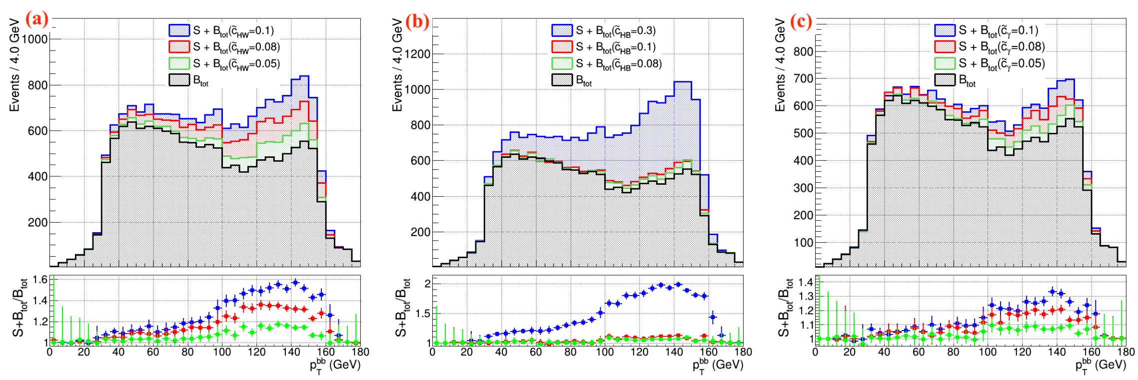

Figure 5.15. Normalized p_T distribution of reconstructed Higgs boson for (a)$\tilde{c}_{HW}$=0.05, 0.08 and 0.1 (b)$\tilde{c}_{HB}$=0.08, 0.1 and 0.3 (c)$\tilde{c}_\gamma$=0.05, 0.08 and 0.1 signals and all total background events at $\sqrt{s}$ = 380 GeV.

Table 5.8. Number of signal for $\tilde{c}_{HW}$=0.1 and relevant backgrounds events after 100 GeV $< H_T <$ 200 GeV cut used for the analysis at $\sqrt{s}$ = 380 GeV with $L_{int} = 1$ ab^{-1} for loosely (90 %) of b-tagging efficiency.

Cuts	$S + B_H$	B_H	B_{ZZ}	B_{tt}	$B_{Z\nu\nu}$	B_{WW}
$\not{E}_T > 30$ GeV	17679	12644	10534	24136	14007	1657
100 GeV $< H_T <$ 200 GeV	16858	11998	8891	7351	11736	1350

Table 5.9. Number of signal for $\tilde{c}_{HW}$=0.1 and relevant backgrounds events after $p_T^{b\bar{b}} >$ 75 GeV cut used for the analysis at $\sqrt{s}$ = 380 GeV with $L_{int} = 1$ ab^{-1} for loosely (90 %) of b-tagging efficiency.

Cuts	$S + B_H$	B_H	B_{ZZ}	B_{tt}	$B_{Z\nu\nu}$	B_{WW}
100 GeV $< H_T <$ 200 GeV	16858	11998	8891	7351	11736	1350
$p_T^{b\bar{b}} >$ 75 GeV	9691	6343	381	1427	417	20

5.3 $\sqrt{s}$ = 1.5 TeV

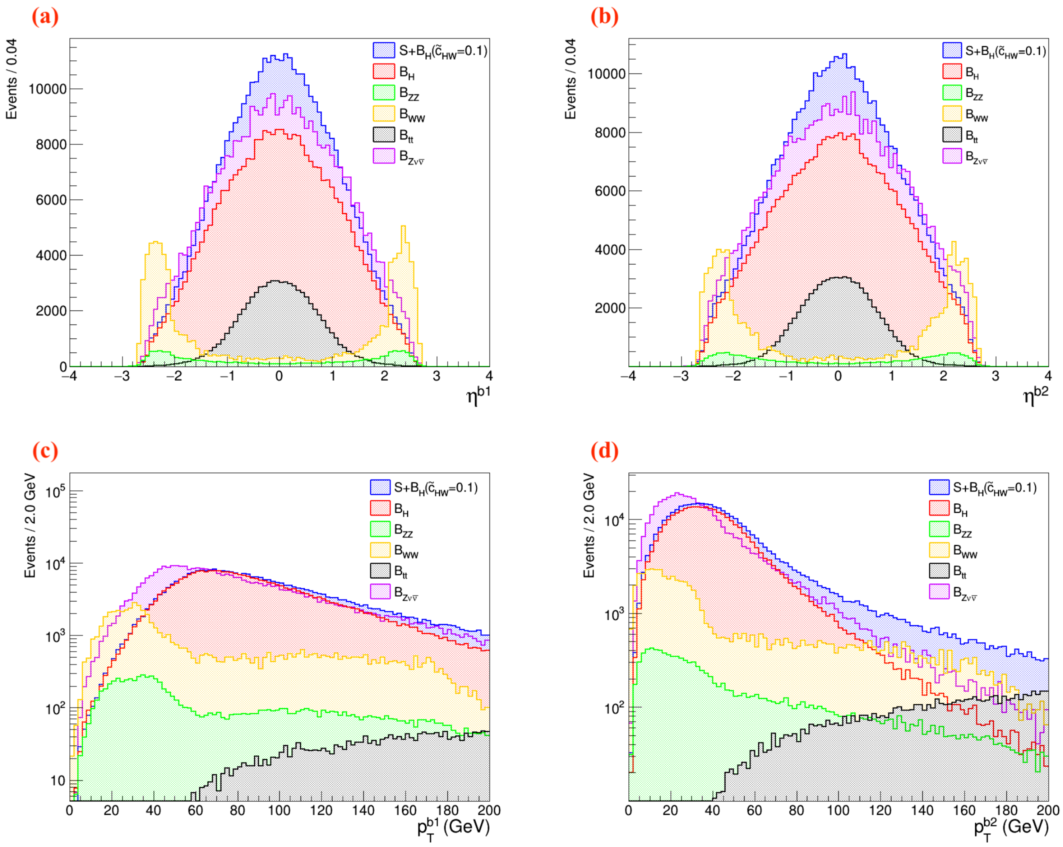

Figure 5.16. Normalized distributions of transverse momentum, pseudo-rapidity of tagged b-jets at $\sqrt{s}$ =1.5 TeV for signal with $\tilde{c}_{HW} = 0.1$ and relevant background processes after cut1.

As in $\sqrt{s}$ = 380 GeV center of mass analysis, same steps had been followed in this section, except for some modifications. First of all, $\tilde{c}_{HW}$= 0.05, 0.08, 0.1, 0.3 and 0.5, $\tilde{c}_{HB}$= 0.05, 0.08, 0.1, 0.3 and 0.5, $\tilde{c}_{\gamma}$= 0.05, 0.08, 0.1, 0.3 and 0.5 signal values were produced.In addition, just 90% working point of b-tagging efficiency was used for the analysis. All the figures that used for this section, were normalized to all process cross sections times integrated luminosity with $L_{int} = 2.5ab^{-1}$. Moreover, in Table 5.1 the cross section values of all relevant were given with respect to increase of the CLIC center of mass energy. As it can be seen from the this table, there are dramatic reduces for cross sections especially for $B_{t\bar{t}}$ and B_{WW} backgrounds. From this and kinematical distributions that we got for this stage, only cut-3 was modified to H_T > 100 GeV.

In this part of the analysis, the reference signal was again $\tilde{c}_{HW}$ = 0.1 and the kinematical distributions which are η^{b_1,b_2} and $p_T^{b_1,b_2}$ were shown (Figure 5.16). From literature, it is known that the density of pseudo-rapidity increases with the increase of particles center of mass energy. In Figure 5.16 the density of pseudo-rapidity was increased in the mass region of reconstructed Higgs boson from two b-jets, compared with $\sqrt{s}$ = 380 GeV analysis. In addition, the behavior of distributions were not changed. So the optimum cut was required to be $|\eta^{b1,b2}| \leq 2.0$. Next, the distributions for transverse momentum of signal and SM background behaved same again with $\sqrt{s}$ = 380 GeV analysis. But the distributions of B_{WW}, B_{ZZ} and $B_{t\bar{t}}$ changed. $p_T^{b_1,b_2}$ cut has been more efficient at 1.5 TeV center of mass energy when compared with the first energy stage of CLIC. Since, the cross section values of these three backgrounds were low, the optimum cut values ($p_T^{b1} > 50$ GeV, $p_T^{b2} > 30$ GeV) were again used like the previous section 5.2 with taken into account the signal and SM background distributions.

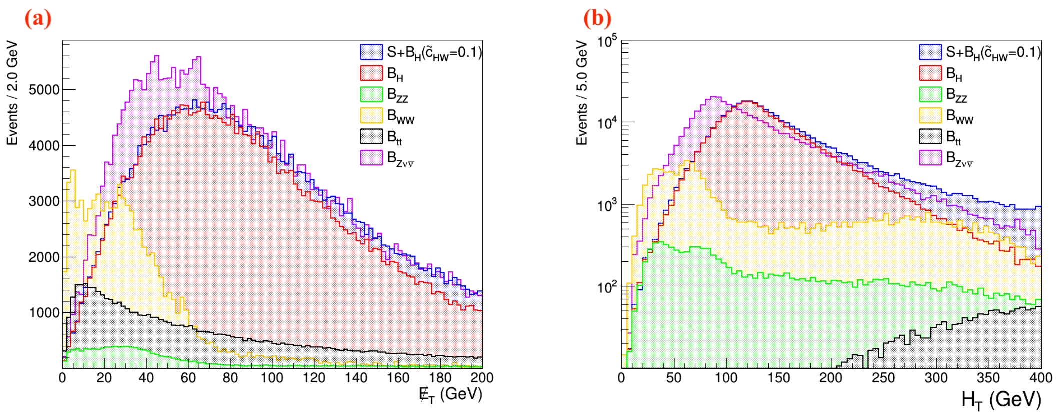

Figure 5.17. Normalized distributions of MET and scalar HT of tagged b-jets at $\sqrt{s}$ =1.5 TeV for signal with $\tilde{c}_{HW} = 0.1$ and relevant background processes after cut1.

In TeV scale the effects of low MET is not so much observed. Due to the reduced cross section values of $B_{t\bar{t}}$, B_{WW} and B_{ZZ} backgrounds, it was not considered these three backgrounds for determining the Cut-2. On the other hand, in order to suppress the $B_{Z\nu\nu}$ background whose cross section increases with the center of mass energy, Cut-2 ($\not{E}_T > 30$ GeV) was carried out (Figure 5.17 (a)). It is well known that while the center of mass energy increases as the cross section of the top quark pair production in e^+e^- collisions decreases. At the same time, considering the distribution in Figure 5.17 (b), Cut-3 was modified to H_T > 100 GeV. Next, in Figure 5.18 shows p_T^{bb} distributions for all couplings with three reference signal after Cut-4. All background events were again suppressed by using optimum cuts for $\sqrt{s}$ = 1.5 TeV center of mass energy of CLIC (Figure 5.18).

Table 5.10. Number of events for $\tilde{c}_{HW}$=0.1 and relevant backgrounds events after $p_T^{b\bar{b}} > 75$ GeV cut used for the analysis at $\sqrt{s}$ = 1.5 TeV with $L_{int} = 2.5$ ab^{-1}.

Cuts	$S + B_H$	B_H	B_{ZZ}	B_{tt}	$B_{Z\nu\nu}$	B_{WW}
100 GeV $< H_T <$ 200 GeV	178677	122339	176.4	70	6325	36
$p_T^{b\bar{b}} > 75$ GeV	157328	100982	176.4	69	5943	36

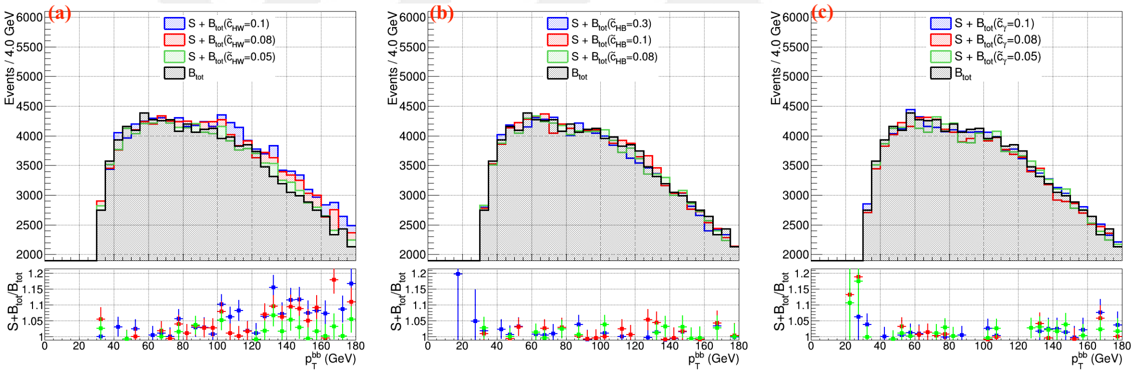

Figure 5.18. Normalized p_T distribution of reconstructed Higgs boson for (a)$\tilde{c}_{HW}$=0.05, 0.08 and 0.1 (b)$\tilde{c}_{HB}$=0.08, 0.1 and 0.3 (c)$\tilde{c}_{\gamma}$=0.05, 0.08 and 0.1 signals and all total background events at $\sqrt{s}$ = 1.5 TeV.

5.4 $\sqrt{s}$ = 3.0 TeV

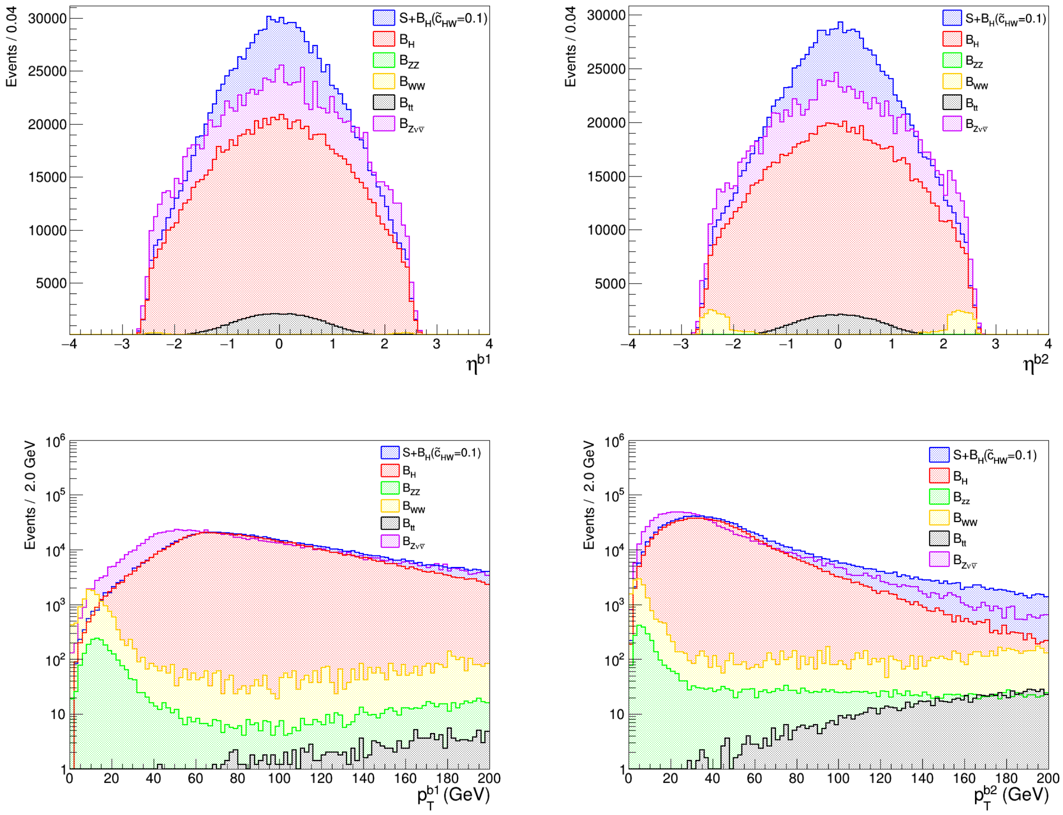

Figure 5.19. Normalized distributions of transverse momentum, pseudo-rapidity of tagged b-jets at $\sqrt{s}$ =3 TeV for signal with $\tilde{c}_{HW} = 0.1$ and relevant background processes after cut1.

As the analysis of first and second energy stages, same steps were following for the analysis of third energy stage of CLIC whose center of mass energy is $\sqrt{s}$ = 3 TeV with considering Figures 5.19 and 5.20. In this part $\tilde{c}_{HW}$ = 0.05, 0.08, 0.1, 0.3, 0.5, $\tilde{c}_{HB}$ = 0.05, 0.08, 0.1, 0.3, 0.5 and $\tilde{c}_{\gamma}$ = 0.05, 0.08, 0.1, 0.3, 0.5 signal events were produced and only 90% b-tagging working point was used like previous section. All distributions were normalized to cross section of processes times integrated luminosity with $L_{int} = 5.0\ ab^{-1}$. As shown in Table 5.1 while the cross section values of $B_{t\bar{t}}$, B_{ZZ} and B_{WW} were reduced drastically, signals and other backgrounds which are SM and $B_{Z\nu\nu}$, were increased. As a result, these effects were seen in the previous analysis so there will be no modification for cut base study in this part.

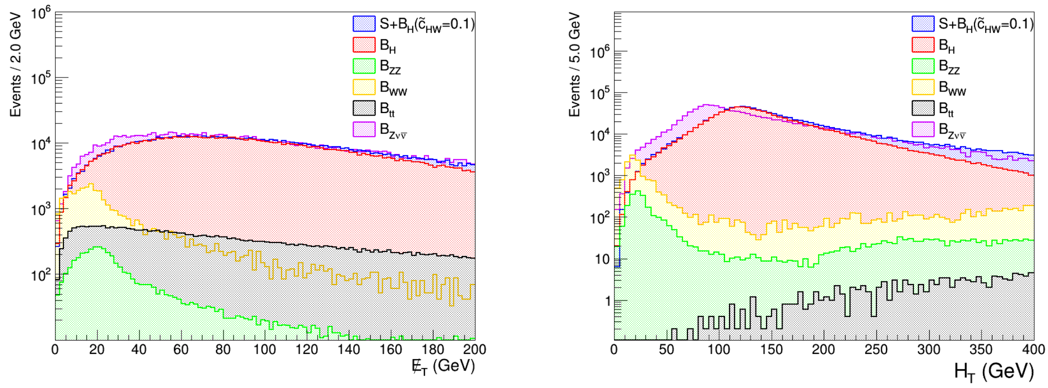

Figure 5.20. Normalized distributions of MET and scalar HT of tagged b-jets at $\sqrt{s}$ =3 TeV for signal with $\tilde{c}_{HW} = 0.1$ and relevant background processes after cut1.

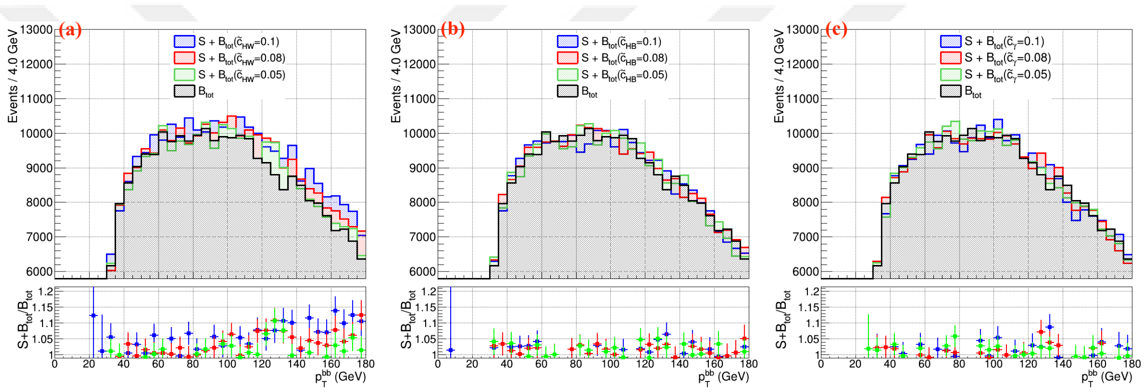

Figure 5.21. Normalized p_T distribution of reconstructed Higgs boson for (a)$\tilde{c}_{HW}$=0.05, 0.08 and 0.1 (b)$\tilde{c}_{HB}$=0.08, 0.1 and 0.3 (c)$\tilde{c}_{\gamma}$=0.05, 0.08 and 0.1 signals and all total background events at $\sqrt{s}$ = 3 TeV.

5.5 Sensitivity of Higgs Gauge Boson Couplings

The sensitivity of dimension-6 CP-violating couplings of the Higgs boson can be calculated with using χ^2 method which express in the following.

$$\chi^2(\tilde{c}) = \sum_{i}^{n_{bins}} \left(\frac{N_i^{NP}(\tilde{c}) - N_i^{B_{tot}}}{N_i^{B_{tot}} \Delta_i} \right)^2 \tag{5.1}$$

Here N^{NP} is the total number of events (S) of signal and all SM backgrounds (B_{tot}), $N^{B_{tot}}$ is the sum of the number of events of all backgrounds ($B_{tot} = B_H + B_{tt} + B_{ZZ} + B_{Z\nu\nu} + B_{WW}$). $\Delta_i = \sqrt{\delta_{sys}^2 + \frac{1}{N_i^B}}$ is representation of combined statistical and systematic errors in each bin. In this thesis, we focused on obtaining limits with 95% confidence level (CL) for $c_{\tilde{H}W}$, $c_{\tilde{H}B}$ and $\tilde{c_\gamma}$ couplings through $e^+e^- \to \nu\bar{\nu}H$ process at different center of mass energies which were $\sqrt{s}$ = 380 GeV, 1.5 TeV, 3 TeV of CLIC with integrated luminosities L_{int}= 1.0 ab^{-1}, 2.5 ab^{-1}, 5.0 ab^{-1} respectively. Furthermore, b-tagging WP was another subject in this analysis because we looked at $H \to bb$ decay channel in final state. Therefore, to compare the effects of three b-tagging WP at first energy stage of CLIC was shown (Figure 5.21). As it is seen from figure, we reached better limits for loose WP (90% b-tagging efficiency) than medium (70% b-tagging efficiency) and tight (50% b-tagging efficiency). Additionally, more percentages of b-tagging efficiency, more sensitivity for CLIC.

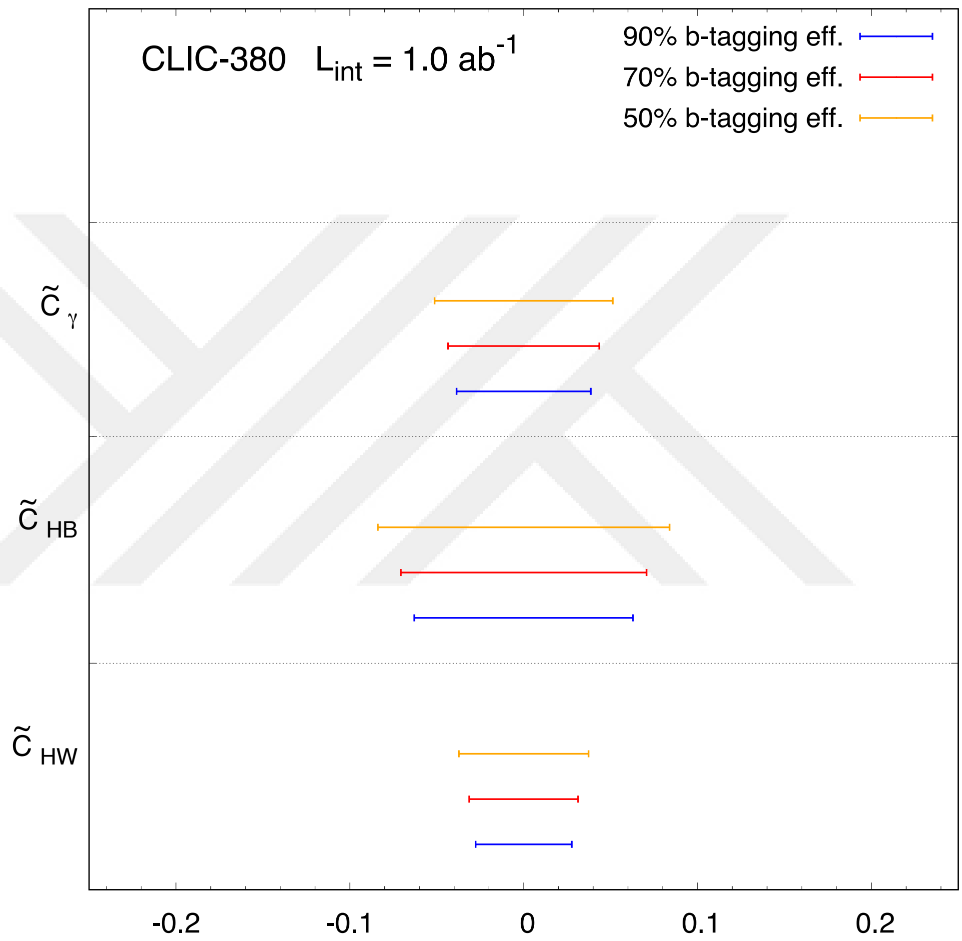

Figure 5.22. Limits comparison of b-tagging efficiencies with three working points at $\sqrt{s}$ = 380 GeV with L_{int}= 1.0 ab^{-1}

Moreover, comparison of obtained limit with 95% CL between three energy stages of CLIC with 90% b-tagging efficiency and HL-LHC was shown (Figure 5.23) (Ferreira et al., 2017). $\tilde{c}_\gamma$ limit of HL-LHC was $[-0.6 \times 10^{-3}; 0.6 \times 10^{-3}]$ via $pp \to h \to \gamma\gamma$ process and also the limits for all three energy stages of CLIC were $[-0.3\times10^{-1}; 0.3\times10^{-1}]$, $[-0.2\times10^{-1}; 0.2\times 10^{-1}]$, $[-1.7 \times 10^{-2}; 1.7 \times 10^{-2}]$. As understand from both limit values and Figure 5.23 the sensitivity of CLIC for $\tilde{c}_\gamma$ coupling, is far from HL-LHC. When looking at $\tilde{c}_{HW}$ results, the limits of each stages of CLIC are $[-2 \times 10^{-2}; 2 \times 10^{-2}]$, $[-1 \times 10^{-2}; 1 \times 10^{-2}]$, $[-7 \times 10^{-3}; 7 \times 10^{-3}]$ respectively and for HL-LHC is $[-6 \times 10^{-2}; 6 \times 10^{-2}]$. In this case the limit values of CLIC was better than HL-LHC in all three energy stages. Especially at $\sqrt{s} = 3$ TeV the limit were low about one order magnitude. In addition, our limits also better than LHC with center of mass energy $\sqrt{s}$ = 13 TeV and L_{int} = 36.1 fb^{-1} as expected. Furthermore, $\tilde{c}_{HB}$ couplings were $[-5 \times 10^{-2}; 5 \times 10^{-2}]$, $[-3.3 \times 10^{-2}; 3.3 \times 10^{-2}]$, $[-3 \times 10^{-2}; 3 \times 10^{-2}]$ for three energy stages of CLIC and $[-2.3 \times 10^{-1}; 3 \times 10^{-1}]$ for HL-LHC. CLIC limits again was better about one order magnitude. In summary, while HL-LHC was more sensitive for $\tilde{c}_\gamma$ coupling, CLIC promises more sensitive for $\tilde{c}_{HW}$, $\tilde{c}_{HB}$ couplings.

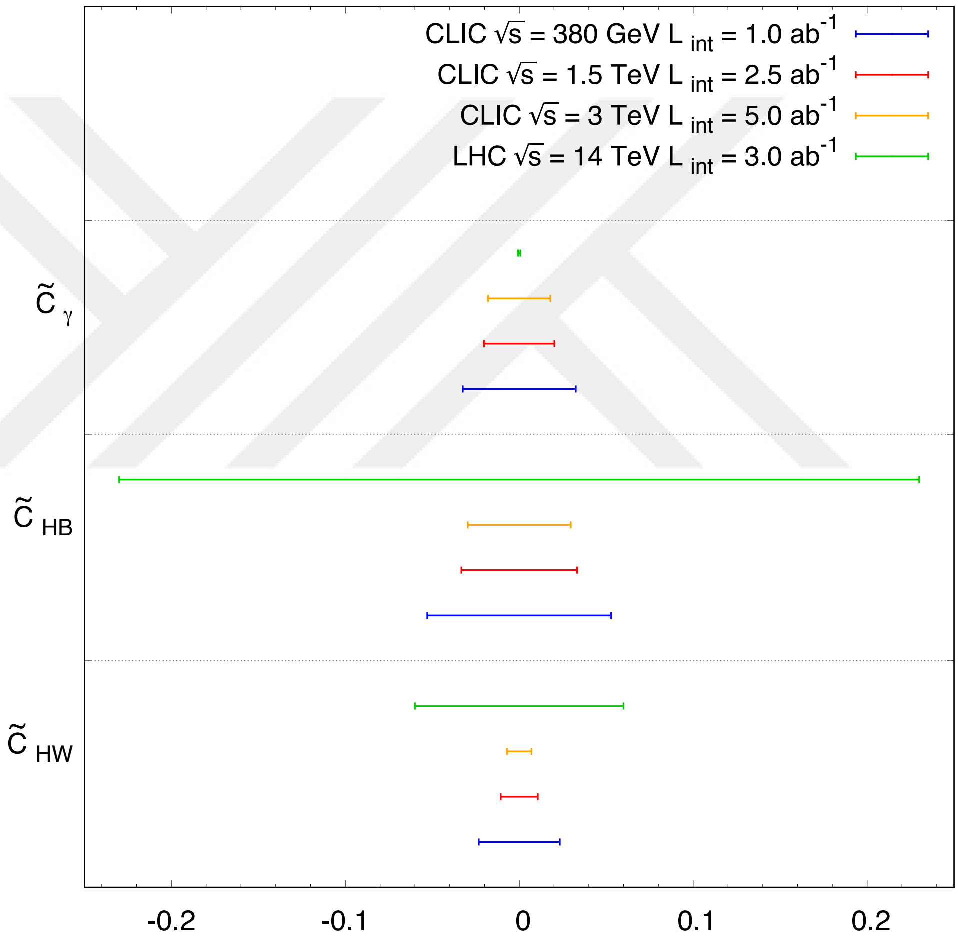

Figure 5.23. Limits comparison for all energy stages of CLIC with 90% b-tagging efficiency and HL-LHC limits at $\sqrt{s}$ = 14 TeV with L_{int}= 3 ab^{-1}

6. CONCLUSION

In this thesis, the phenomenon of CP-violation in the Higgs sector, is studied within the framework of NP BSM. With using SM EFT approach in $e^+e^- \to \nu\bar{\nu}H$ process , dimension-6 CP violating operators were defined and the effects of these operators were focused. The relevant backgrounds determined with respect to the final state of the signal ($H \to bb$). With 3 different working points for b-tagging efficiency, signals and backgrounds were produced by considering the realistic detector effects with the tuned CLIC detector card designed for three energy stage of CLIC. With considering the kinematical distributions for these events, cut base study was done and dominant backgrounds were suppressed. Then the limits with 95% CL, calculated for $\tilde{c}_{HW}$, $\tilde{c}_{HB}$ and $\tilde{c}_{\gamma}$ couplings which contained CP-violating contributions, with the integral values of invariant mass distributions of the Higgs reconstructed from b-jet pairs.

As a result of this thesis, for all energy stages, CLIC is promising more sensitive results for $\tilde{c}_{HW}$ and $\tilde{c}_{HB}$ couplings than other dimension-6 CP-violating operators . In addition, when comparing the sensitivity of three energy stages of CLIC with HL-LHC and current experiment LHC, even in first energy stage of CLIC gives precision measurements for $\tilde{c}_{HW}$ and $\tilde{c}_{HB}$ couplings. Finally, CLIC with its clean environment is a good option among future accelerators to understand the CP violation in BSM and many other physical phenomenons.

REFERENCES

Aaboud M et al. (2018) “Measurements of Higgs boson properties in the diphoton decay channel with 36 fb^{-1} of pp collision data at $\sqrt{s} = 13$ TeV with the ATLAS detector”, Phys. Rev., D98:052005.

Aad G et al. (2012) “Observation of a new particle in the search for the standard model higgs boson with the ATLAS detector at the LHC”, Phys.Lett., B716:1–29.

Aad G et al. (2016) “Constraints on non-Standard Model Higgs boson interactions in an effective Lagrangian using differential cross sections measured in the $H \to \gamma\gamma$ decay channel at $\sqrt{s} = 8$TeV with the ATLAS detector”, Phys. Lett., B753:69–85.

Abachi S, Abbott B, Abolins M, Acharya B S, Adam I, Adams D L, Adams M, Ahn S, Aihara H, Alitti J, and et al (1995) “Observation of the top quark”, Physical Review Letters, 74(14):2632–2637.

Aicheler M, Burrows P, Draper M, Garvey T, Lebrun P, Peach K, Phinney N, Schmickler H, Schulte D, and Toge N (2012) A Multi-TeV Linear Collider Based on CLIC Technology: CLIC Conceptual Design Report, CERN Yellow Reports: Monographs, CERN, Geneva.

Alloul A, Christensen N D, Degrande C, Duhr C, and Fuks B (2014a) “FeynRules 2.0 - A complete toolbox for tree-level phenomenology”, Comput. Phys. Commun., 185:2250–2300.

Alloul A, Fuks B, and Sanz V (2014b) “Phenomenology of the Higgs Effective Lagrangian via FEYNRULES”, JHEP, 04:110.

Alwall J, Frederix R, Frixione S, Hirschi V, Maltoni F, Mattelaer O, Shao H S, Stelzer T, Torrielli P, and Zaro M (2014) “The automated computation of tree-level and next-to-leading order differential cross sections, and their matching to parton shower simulations”, JHEP, 07:079.

Amar G, Banerjee S, von Buddenbrock S, Cornell A S, Mandal T, Mellado B, and Mukhopadhyaya B (2015) “Exploration of the tensor structure of the Higgs boson coupling to weak bosons in e^+e^- collisions”, Journal of High Energy Physics, 2015(2).

Bardon M, Lande K, Lederman L, and Chinowsky W (1958) “Long-lived neutral K mesons”, Annals Physics, 5(2):156–181.

Beneke M, Boito D, and Wang Y M (2014) “Anomalous Higgs couplings in angular asymmetries of $H \to Z\ell^+\ell^-$ and e$^+$ e$^-$ $\to HZ$”, JHEP, 11:028.

Bernlochner F U, Englert C, Hays C, Lohwasser K, Mildner H, Pilkington A, Price D D, and Spannowsky M (2019) “Angles on CP-violation in Higgs boson interactions”, Phys. Lett., B790:372–379.

Biswal S S and Godbole R M (2009) “Use of transverse beam polarization to probe anomalous VVH interactions at a Linear Collider”, Phys. Lett., B680:81–87.

Biswal S S, Godbole R M, Mellado B, and Raychaudhuri S (2012) “Azimuthal Angle Probe of Anomalous HWW Couplings at a High Energy ep Collider”, Phys. Rev. Lett., 109:261801.

Boronat M, Fuster J, Garcia I, Ros E, and Vos M (2015a) “A robust jet reconstruction algorithm for high-energy lepton colliders”, Phys. Lett., B750:95–99.

Boronat M, Fuster J, García I, Ros E, and Vos M (2015b) “A robust jet reconstruction algorithm for high-energy lepton colliders”, Physics Letters B, 750:95–99.

Branco G, Ferreira P, Lavoura L, Rebelo M, Sher M, and Silva J P (2012) “Theory and phenomenology of two-higgs-doublet models”, Physics Reports, 516(1-2):1–102.

Brod J, Haisch U, and Zupan J (2013) “Constraints on CP-violating Higgs couplings to the third generation”, JHEP, 11:180.

Brun R and Rademakers F (1997) “ROOT: An object oriented data analysis framework”, Nucl. Instrum. Meth., A389:81–86.

Cabibbo N (1963) “Unitary Symmetry and Leptonic Decays”, Phys. Rev. Lett., 10:531–533, [,648(1963)].

Cacciari M, Salam G P, and Soyez G (2012) “FastJet User Manual”, Eur. Phys. J., C72:1896.

Ceccucci A, Ligeti Z, and Sakai Y (2018) “CKM quark-mixin matrix”, http://pdg.lbl.gov/2019/reviews/rpp2019-rev-ckm-matrix.pdf, 15-02-2020.

Cepeda M et al. (2019) “Higgs physics at the hl-lhc and he-lhc”, https://arxiv.org/abs/1902.00134, 20-05-2020.

Charles T K et al. (2018) “The Compact Linear Collider (CLIC) - 2018 Summary Report”, CERN Yellow Rep. Monogr., 1802:1–98.

Chatrchyan S et al. (2012) “Observation of a new boson at a mass of 125 gev with the CMS experiment at the LHC”, Phys. Lett., B716:30–61.

Christenson J H, Cronin J W, Fitch V L, and Turlay R (1964) “Evidence for the 2π decay of the k_2^0 meson”, Phys. Rev. Lett., 13:138–140.

Contino R, Ghezzi M, Grojean C, Muhlleitner M, and Spira M (2013) “Effective Lagrangian for a light Higgs-like scalar”, JHEP, 07:035.

Cowan C L, Reines F, Harrison F B, Kruse H W, and McGuire A D (1956) “Detection of the free neutrino: a confirmation”, Science, 124(3212):103–104.

de Favereau J, Delaere C, Demin P, Giammanco A, Lemaître V, Mertens A, and Selvaggi M (2014) “DELPHES 3, A modular framework for fast simulation of a generic collider experiment”, JHEP, 02:057.

Degrande C, Duhr C, Fuks B, Grellscheid D, Mattelaer O, and Reiter T (2012) “UFO - The Universal FeynRules Output”, Comput. Phys. Commun., 183:1201–1214.

Desai N, Ghosh D K, and Mukhopadhyaya B (2011) “CP-violating HWW couplings at the Large Hadron Collider”, Phys. Rev., D83:113004.

Dwivedi S, Ghosh D K, Mukhopadhyaya B, and Shivaji A (2016) “Distinguishing CP-odd couplings of the Higgs boson to weak boson pairs”, Phys. Rev., D93:115039.

Einstein A (1905) “On the electrodynamics of moving bodies”, Annalen Phys., 17:891–921.

ExRootAnalysis (1999) “ExRootAnalysis”, http://madgraph.physics.illinois.edu/Downloads/ExRootAnalysis/, 2020-05-27.

Ferreira F, Fuks B, Sanz V, and Sengupta D (2017) “Probing CP-violating Higgs and gauge-boson couplings in the Standard Model effective field theory”, Eur. Phys. J., C77(10):675.

Gell-Mann M (1957) “Model of the strong couplings”, Phys. Rev., 106:1296–1300.

Giudice G F, Grojean C, Pomarol A, and Rattazzi R (2007) “The Strongly-Interacting Light Higgs”, JHEP, 06:045.

Godbole R, Miller D J, Mohan K, and White C D (2014) “Boosting Higgs CP properties via VH Production at the Large Hadron Collider”, Phys. Lett., B730:275–279.

Gorbunov D S and Rubakov V A (2011) Introduction To The Theory Of The Early Universe: Hot Big Bang Theory, World Scientific Publishing Company.

Kobayashi M and Maskawa T (1973) “CP Violation in the Renormalizable Theory of Weak Interaction”, Prog. Theor. Phys., 49:652–657.

Kumar S, Poulose P, and Sahoo S (2015) “Study of Higgs-gauge boson anomalous couplings through $e^-e^+ \to W^-W^+H$ at ILC”, Phys. Rev., D91(7):073016.

Leogrande E, Roloff P, Schnoor U, and Weber M (2019) “A DELPHES card for the CLIC detector”, https://arxiv.org/abs/1909.12728, 15-03-2020.

Linssen L, Miyamoto A, Stanitzki M, and Weerts H (2012) “Physics and detectors at clic: Clic conceptual design report”, https://arxiv.org/abs/1202.5940, 15-03-2020.

LLC M (2018) “Cronin and Fitch Experiment with Kaons”, http://hyperphysics.phy-astr.gsu.edu/hbase/Particles/cronin.html, 10-02-2020.

Millikan R A (1913) “On the elementary electrical charge and the avogadro constant”, Phys. Rev., 2:109–143.

Neddermeyer S H and Anderson C D (1937) “Note on the nature of cosmic-ray particles”, Phys. Rev., 51:884–886.

Rao K and Rindani S D (2006) “Probing CP-violating contact interactions in e+ e- —> HZ with polarized beams”, Phys. Lett., B642:85–92.

Robson A and Roloff P (2018) “Updated CLIC luminosity staging baseline and Higgs coupling prospects”, https://arxiv.org/abs/1812.01644, 15-03-2020.

Roloff P, Franceschini R, Schnoor U, and Wulzer A (2018) “The Compact Linear e^+e^- Collider (CLIC): Physics Potential”, https://arxiv.org/abs/1812.07986, 15-03-2020.

Sirunyan A, Tumasyan A, Adam W, Ambrogi F, Asilar E, Bergauer T, Brandstetter J, Dragicevic M, Erö J, Escalante Del Valle A, and et al (2019a) “Measurements of the higgs boson width and anomalous hvv couplings from on-shell and off-shell production in the four-lepton final state”, Physical Review D, 99(11).

Sirunyan A M et al. (2019b) “Constraints on anomalous HVV couplings from the production of Higgs bosons decaying to τ lepton pairs”, Submitted to: Phys. Rev.

Sjöstrand T, Ask S, Christiansen J R, Corke R, Desai N, Ilten P, Mrenna S, Prestel S, Rasmussen C O, and Skands P Z (2015) “An introduction to pythia 8.2”, Computer Physics Communications, 191:159–177.

Street J C and Stevenson E C (1937) “New evidence for the existence of a particle of mass intermediate between the proton and electron”, Phys. Rev., 52:1003–1004.

Tuning N (2020) “Lectures Notes on CP-violation ”, https://www.nikhef.nl/~h71/Lectures/2015/ppII-cpviolation-29012015.pdf, 02-02-2020.

Wolfenstein L (1983) “Parametrization of the kobayashi-maskawa matrix”, Phys. Rev. Lett., 51:1945–1947.

CURRICULUM VITAE

Name Surname	: Özgün KARADENİZ
Place and Date of Birth	: DÜZCE, 29.06.1988
University	
Bachelor's Degree	: Bolu Abant İzzet Baysal University,
e-mail	: ozgunkdz@gmail.com ozgun.karadeniz@cern.ch
Address	: Çiftepınarlar Mahallesi Huzur Evler Sitesi A-3 Blok Daire-7 DÜZCE/Merkez
Projects	: The Scientific and Technological Research Council of Turkey, Grant No:118F333 Turkish Atomic Energy Authority (TAEK) under the Grant No. 2018 TAEK (CERN) A5.H6.F2-20
List of Publications	: O. KARADENİZ, A. ŞENOL, K. Y. OYULMAZ, H. DENİZLİ "CP-Violating Higgs-gauge boson couplings in $H\nu\bar{\nu}$ production at three energy stages of CLIC." The European Physical Journal C, 2020. A. ŞENOL, H. DENİZLİ, A. YILMAZ K. Y. OYULMAZ, O. KARADENİZ, O. ÇAKIR "Probing the effects of dimension-eight operators describing anomalous neutral triple gauge boson interactions at FCC-hh Nuclear Physics B, 2018.
Awards	: Academic Encouragement Award, Bolu Abant Izzet Baysal University, Bolu, Turkey, 2018